Aalto University School of Science and Technology
Inorganic Chemistry Publication Series
Espoo 2010 No. 11

HIGH-κ TERNARY RARE EARTH OXIDES BY ATOMIC LAYER DEPOSITION

Doctoral Dissertation

Pia Myllymäki

Dissertation for the degree of Doctor of Science in Technology to be presented with due permission of the Faculty of Chemistry and Materials Sciences for public examination and debate in Auditorium KE 2 at Aalto University School of Science and Technology (Espoo, Finland) on the 8th of December, 2010, at 12 noon.

Aalto University
School of Science and Technology
Faculty of Chemistry and Materials Sciences
Department of Chemistry

Aalto-yliopisto
Teknillinen korkeakoulu
Kemian ja materiaalitekniikan tiedekunta
Kemian laitos

Supervisor:

Prof. Maarit Karppinen
Laboratory of Inorganic Chemistry
Aalto University School of Science and Technology

Pre-examiners:

Prof. Jaan Aarik
Institute of Physics
University of Tartu, Estonia

Prof. Anders Hårsta
Department of Materials Chemistry
The Ångström Laboratory
Uppsala University, Sweden

Opponent:

Prof. Mikko Ritala
Laboratory of Inorganic Chemistry
Department of Chemistry
University of Helsinki, Finland

Distribution:

Aalto University
School of Science and Technology
Faculty of Chemistry and Materials Sciences
Department of Chemistry
P.O.Box 16100
FI-00076 Aalto
FINLAND
E-mail: piitu.myllymaki@gmail.com

ISBN 978-952-60-3488-1 (print)
ISBN 978-952-60-3489-8 (PDF)
ISSN 1458-5154
URL: http://lib.tkk.fi/Diss/2010/isbn9789526034898

Multiprint Oy
Espoo 2010

Aalto University

ABSTRACT OF DOCTORAL DISSERTATION	AALTO UNIVERSITY SCHOOL OF SCIENCE AND TECHNOLOGY P.O. BOX 11000, FI-00076 AALTO http://www.aalto.fi

Author Pia Myllymäki

Name of the dissertation
High-κ ternary rare earth oxides by atomic layer deposition

Manuscript submitted 15.09.2010	Manuscript revised
Date of the defence 08.12.2010	
☐ Monograph	☒ Article dissertation (summary + original articles)

Faculty	Faculty of Chemistry and Materials Sciences
Department	Department of Chemistry
Field of research	Inorganic Chemistry
Opponent(s)	Prof. Mikko Ritala
Supervisor	Acad. Prof. Maarit Karppinen
Instructor	Prof. (emer.) Lauri Niinistö, Ma. Prof. Matti Putkonen

The present thesis describes atomic layer deposition (ALD) of ternary rare earth (RE) oxides and characterization of compositional, structural and electrical properties of the films. The $REScO_3$, $LaLuO_3$ and $Er_xGa_{2-x}O_3$ thin films investigated are potential high-κ materials for future metal-oxide-semiconductor field-effect transistors, *i.e.* MOSFETs. The dissertation consists of five peer reviewed publications.

As a background for the work, issues related to the miniaturization of MOSFETs and the feasibility of rare earth oxides as new high-κ dielectrics are discussed. Also some challenges of manufacturing Ga-based MOSFETs with high quality gate oxide having satisfactory interface properties and the role of rare earth oxides in GaAs passivation are presented. In addition the basic principle of the ALD method is briefly introduced and recent literature concerning deposition of rare earth oxides is reviewed.

A series of $REScO_3$ thin films was deposited by ALD using rare earth β-diketonate precursors $RE(thd)_3$ together with ozone. The films were characterized for growth rate, elemental composition, crystallization upon annealing and electrical properties. Amorphous films of high quality with low impurity contents and promising electrical characteristics were produced. Several gradually evolving properties of the films were examined and the effect of the RE^{3+} cation size was discussed. $YScO_3$ films were also deposited using novel cyclopentadienyl metal precursors and water. Deposition of $LaLuO_3$ films having similar properties but even higher dielectric constant (κ ≈ 30) than ternary scandates was examined at two different temperatures. The relationship between the crystallization behaviour and the dielectric constant of $REScO_3$ and $LaLuO_3$ thin films was discussed. Finally deposition of a possible gate oxide for GaAs MOSFETs, *viz.* $Er_xGa_{2-x}O_3$ by two different precursor approaches was investigated. In addition to β-diketonate metal precursors novel cyclopentadienyl and amidinate metal precursors together with water as oxygen source were utilized. For both $YScO_3$ and $Er_xGa_{2-x}O_3$ films the choice of precursor system affected *e.g.* the electrical properties and the crystallization behavior.

Keywords thin film, ternary rare earth oxide, high-k dielectric

ISBN (printed) 978-952-60-3488-1	ISSN (printed) 1458-5154
ISBN (pdf) 978-952-60-3489-8	ISSN (pdf) 1458-5154
Language English	Number of pages 50+29 (app.)
Publisher Department of Inorganic Chemistry	
Print distribution Laboratory of Inorganic Chemistry, P.O.Box 16100, 00076 Aalto, Finland	
☒ The dissertation can be read at http://lib.tkk.fi/Diss/2010/isbn9789526034898	

Aalto-yliopisto

VÄITÖSKIRJAN TIIVISTELMÄ	AALTO-YLIOPISTO TEKNILLINEN KORKEAKOULU PL 11000, 00076 AALTO http://www.aalto.fi
Tekijä Pia Myllymäki	
Väitöskirjan nimi Korkean dielektrisen vakion ternääriset harvinaisten maametallien oksidit atomikerroskasvatusmenetelmällä	
Käsikirjoituksen päivämäärä 15.09.2010	Korjatun käsikirjoituksen päivämäärä
Väitöstilaisuuden ajankohta 08.12.2010	
☐ Monografia	☒ Yhdistelmäväitöskirja (yhteenveto + erillisartikkelit)

Tiedekunta	Kemian ja materiaalitieteiden tiedekunta
Laitos	Kemian laitos
Tutkimusala	Epäorgaaninen kemia
Vastaväittäjä(t)	Prof. Mikko Ritala
Työn valvoja	Akat. Prof. Maarit Karppinen
Työn ohjaaja	Prof. (emer.) Lauri Niinistö, Ma. Prof. Matti Putkonen

Tässä väitöskirjassa esitetään harvinaisten maametallien (RE) ternääristen oksidiohutkalvojen kasvatus atomikerroskasvatusmenetelmällä (ALD) ja kalvojen koostumuksen, rakenteen ja sähköisten ominaisuuksien karakterisointi. Työssä tutkittujen $REScO_3$-, $LaLuO_3$- ja $Er_xGa_{2-x}O_3$-ohutkalvojen dielektrisyysvakio (κ) on korkea ja sen vuoksi niitä voidaan mahdollisesti käyttää tulevaisuuden metalli-oksidi-puolijohde kenttävaikutustransistorien (MOSFET) hilaoksideina.

Työssä tarkastellaan MOSFET-transistorien koon pienentymiseen liittyviä ongelmia ja pohditaan harvinaisten maametallioksidien soveltuvuutta uusiksi hilaoksideiksi. Lisäksi tarkastellaan lyhyesti Ga-pohjaisten MOSFET-komponenttien ja erityisesti korkealaatuisen hilaeristeen valmistuksen haasteita sekä harvinaisten maametallien oksidien käyttöä GaAs-pinnan passivointiin. Työssä esitetään lyhyesti ALD-menetelmän periaate ja yhteenveto kirjallisuudessa esiintyvistä harvinaisten maametallioksidien tutkimuksista.

Sarja $REScO_3$-ohutkalvoja kasvatettiin käyttämällä lähdeaineina harvinaisten maametallien β-diketonaattiyhdisteitä, $RE(thd)_3$ ja otsonia. Kalvot olivat amorfisia ja korkealaatuisia sisältäen vain pieniä määriä epäpuhtauksia. Kalvojen sähköiset ominaisuudet olivat lupaavia elektroniikan sovellutusten kannalta. Ohutkalvojen kasvunopeudet määritettiin sekä kalvojen kemiallista koostumusta, kiteytymistä lämpökäsittelyissä sekä sähköisiä ominaisuuksia tutkittiin. Kasvatuksen jälkeen kalvot olivat korkealaatuisia, rakenteeltaan amorfisia, ja sisälsivät vain pienen määrän epäpuhtauksia. Tutkimuksessa havaittiin, että useat ohutkalvojen ominaisuudet muuttuvat vaiheittain RE^{3+}-kationin koon muuttuessa. $YScO_3$-ohutkalvoja kasvatettiin myös käyttäen lähdeaineina syklopentadienyyliyhdisteitä ja vettä. $LaLuO_3$-ohutkalvoja kasvatettiin kahdessa eri lämpötilassa ja havaittiin, että niillä on useita samanlaisia ominaisuuksia kuin $RESCO_3$-ohutkalvoilla, mutta korkeampi dielektrinen vakio (κ ≈ 30). Työssä esitetään $RESCO_3$- ja $LaLuO_3$-ohutkalvojen kiteytymisen vaikutus kalvojen dielektrisyysvakioon. $Er_xGa_{2-x}O_3$-ohutkalvoja, joita voidaan käyttää mahdollisesti GaAs MOSFET-transistoreissa hilaoksidina, kasvatettiin käyttämällä kahta erilaista prosessia; β-diketonaattiyhdisteiden lisäksi käytettiin syklopentadienyyli- ja amidinaattiyhdisteitä metallilähdeaineina sekä vettä hapen lähdeaineena. Sekä $YScO_3$- että $Er_xGa_{2-x}O_3$-ohutkalvoilla lähdeaineiden valinta vaikutti mm. kalvojen sähköisiin ominaisuuksiin sekä kiteytymiseen.

Asiasanat	Ohutkalvo, ternäärinen oksidi, harvinaiset maametallit, hilaoksidi		
ISBN (painettu)	978-952-60-3488-1	ISSN (painettu)	1458-5154
ISBN (pdf)	978-952-60-3489-8	ISSN (pdf)	1458-5154
Kieli	Englanti	Sivumäärä	50+29 (liitteet)
Julkaisija	Kemian laitos		
Painetun väitöskirjan jakelu	Epäorgaanisen kemian laboratorio, PL 16100, 00076 Aalto		
☒ Luettavissa verkossa osoitteessa http://lib.tkk.fi/Diss/2010/isbn9789526034898			

PREFACE

The work presented in this thesis was carried out in the Laboratory of Inorganic Chemistry at Aalto University School of Science and Technology (TKK) between August 2002 and May 2010.

I would like to express my gratitude to Prof. Lauri Niinistö for the opportunity to work in his ALD group and for his endless support and guidance during this time. He introduced me to the world of rare earths and his comments and expert help have been invaluable.

I was very fortunate to have two instructors to guide me during these years. The help of Dr. Minna Nieminen was especially important to me in the beginning and in the end of this journey. Together with Prof. Maarit Karppinen she made sure I would actually finish this thesis. I would also like to thank Dr. Matti Putkonen for many fruitful conversations, valuable suggestions, and also for finding me the perfect bicycle... I'd like to thank all the co-authors for their contributions, especially Dr. Charles Dezelah, Dr. Jaakko Niinistö and Dr. Jani Päiväsaari. Warm thanks to all the co-workers at the Laboratory of the Inorganic Chemistry are in order.

I am grateful for the opportunity to co-operate with Dr. Jürgen Schubert and his group of physicists, especially Dr. Martin Roeckerath and Dr. Joao Marcelo Lopes at the Research Center Jülich, Germany. Without their expertise the characterization of many of the thin films would not have been possible. I want to thank Dr. Timo Sajavaara, Dr. Kai Arstila and Mr. Kenichiro Mizohata for the TOF-ERDA measurements and Dr. Kaupo Kukli for helping with the electrical characterization of thin films.

I wish to thank my parents and sisters Sari and Laura for their support. To the wonderful, crazy group of ladies chasing after the small plastic ball (also known as the Westend Indians Naiset), thank you for keeping me sane and helping me forget the troubles at work during the countless hours of training and having a blast together.

Finally, thank you Tuomas for always, always being there.

Financial support from the Graduate School of Inorganic Materials Chemistry and the Finnish Foundation for Technology Promotion (TES) is gratefully acknowledged.

Espoo, November 2010

Pia Myllymäki

CONTENTS

LIST OF PUBLICATIONS

I P. Myllymäki, M. Nieminen, J. Niinistö, M. Putkonen, K. Kukli, L. Niinistö, High-permittivity $YScO_3$ thin films by atomic layer deposition using two precursor approaches, *J. Mater. Chem.* **16** (2006) 563–569.

II P. Myllymäki, M. Roeckerath, M. Putkonen, S. Lenk, J. Schubert, L. Niinistö, S. Mantl, Characterization and electrical properties of high-κ $GdScO_3$ thin films grown by atomic layer deposition, *Appl. Phys. A* **88** (2007) 633-637.

III P. Myllymäki, M. Roeckerath, J.M. Lopes, J. Schubert, K. Mizohata, M. Putkonen, L. Niinistö, Rare earth scandate thin films by atomic layer deposition: effect of the rare earth cation size, *J. Mater. Chem.* **20** (2010) 4207–4212.

IV M. Roeckerath, T. Heeg, J.M.J. Lopes, J. Schubert, S. Mantl, A. Besmehn, P. Myllymäki, L. Niinistö, Characterization of lanthanum lutetium oxide thin films grown by atomic layer deposition as an alternative gate dielectric, *Thin Solid Films* **517** (2008) 201-203.

V C.L. Dezelah, P. Myllymäki, J. Päiväsaari, K. Arstila, L. Niinistö, C.H. Winter, The growth of $Er_xGa_{2-x}O_3$ films by atomic layer deposition from two different precursor systems, *J. Mater. Chem.* **17** (2007) 1308-1315.

THE AUTHOR'S CONTRIBUTION

Publication I	The author defined the research plan together with co-authors, carried out the thin film depositions together with Dr. Minna Nieminen and did the characterizations excluding TOF-ERDA, AFM and electrical characterization. The author had a major role in writing the manuscript.
Publication II	The author defined the research plan together with co-authors, carried out the thin film depositions and did the characterizations excluding RBS, XRR, SE, AFM, TEM and electrical characterization. The author had a major role in writing the manuscript.
Publication III	The author defined the research plan, carried out the thin film depositions and did the characterizations excluding TOF-ERDA, RBS, XRR, GIXRD and electrical characterization. The author wrote the manuscript.
Publication IV	The author carried out the thin film depositions and had a minor role in writing the manuscript.
Publication V	The author defined the research plan together with Dr. Charles Dezelah and was responsible for the depositions and characterization of thin films grown from the β-diketonate precursors, excluding TOF-ERDA, RBS, XRR, AFM and electrical characterization. The author had a minor role in writing the manuscript.

LIST OF ABBREVIATIONS

acac	Acetyl acetonato, 2,4-pentanedionato
AFM	Atomic Force Microscopy
ALD	Atomic Layer Deposition
amd	Amidinate
bipy	Bipyridine
CET	Capacitance Equivalent Thickness
CMOS	Complementary Metal Oxide Semiconductor
Cp	Cyclopentadienyl
CVD	Chemical Vapor Deposition
EBE	Electron Beam Evaporation
EOT	Equivalent Oxide Thickness
FTIR	Fourier Transform Infrared Spectroscopy
GGG	Gadolinium Gallium Garnet
GIXRD	Grazing Incidence X-Ray Diffraction
MBD	Moleculas Beam Deposition
MBE	Molecular Beam Epitaxy
MOCVD	Metal-Organic Chemical Vapor Deposition
MOS	Metal-Oxide-Semiconductor
MOSFET	Metal-Oxide-Semiconductor Field-Effect Transistor
Phen	1,10-Phenantroline
PLD	Pulsed Laser Deposition
RBS	Rutherford Backscattering spectrometry
RE	Rare earth
SE	Spectroscopic Ellipsometry
TEM	Transmission Electron Microscopy
thd	2,2,6,6-Tetramethyl-3,5-heptanedionate
TOF-ERDA	Time-of-Flight Elastic Recoil Detection Analysis
XRD	X-Ray Diffraction
XRF	X-Ray Fluorescence Spectroscopy
XRR	X-Ray Reflectometry

LIST OF SYMBOLS

A	Capacitor area
C	Capacitance
$C_{d,inv}$	Capacitance density at inversion
C_{max}	Capacitance density at accumulation
D_{it}	Density of interface states
ΔV_{fb}	Hysteresis
ε_0	Permittivity of free space
I_D	Drain current, drive current
κ	Dielectric constant
L	Channel length
μ_{eff}	Effective channel carrier mobility
t	Thickness
W	Channel width
V_D	Drain voltage
V_{fb}	Flat band voltage
V_G	Gate voltage
V_{th}	Threshold voltage

1. Introduction

Wherever we look, we encounter computers; they run our cars, wash our laundry and keep the airplanes in the air. Mobile phones and laptops are not luxury products anymore but a necessity for most of us. The development of computers from the first generation building or room-sized devices to home computers of the 80s and modern day versatile and portable personal communicators has been astonishingly rapid.

Metal-oxide-semiconductor field-effect transistor or MOSFET is the key component in any modern electronic device. MOSFET took over the bipolar junction transistor in the 70s as it came evident that MOSFET technology would make integrated circuit processing simpler and that more components could be packed on a single chip. This has led to continuous downscaling of MOSFETs and exponential growth of the number of transistors on a chip. Traditional SiO_2 gate oxide (dielectric constant $\kappa = 3.9$) has already been replaced in the latest microprocessors by atomic layer deposited hafnium-based gate insulator with higher κ.[1] However, the search for the next generation high-κ insulating materials is an ongoing task.

The rare earth elements (RE), *i.e.* lanthanoids, yttrium and scandium, form a very interesting and coherent group of elements with many similar properties. They are in fact the largest homogeneous group in the periodic table. Due to the gradual reduction in the cation size within the lanthanoid series, *i.e.* the lanthanoid contraction, many properties gradually change within the lanthanoid group. Yttrium is similar in size with the heavier lanthanoids erbium and holmium while scandium is the smallest of the group. With a few exceptions, their most stable, and in many cases the only, oxidation state is +3. Rare earth oxides and especially ternary rare earth scandates $RESCO_3$ have recently gained considerable attention as possible high-κ gate oxides.[2,3] They have high dielectric constant and large band gap and offset to silicon. Especially $GdScO_3$[II,4] and $DyScO_3$[III,5-7] have been widely studied. An n-MOSFET with $GdScO_3$ gate oxide on strained silicon with excellent properties (*viz.* low leakage current density, high I_{on}/I_{off} ratio and large carrier mobility) has been recently demonstrated.[8]

Replacing the SiO_2 with another gate oxide material is not a straightforward task. Traditionally SiO_2 gate oxide has been produced by thermal oxidation of the silicon substrate. Obviously with new materials different processes must be applied. Atomic Layer Deposition (ALD) method, which is

based on sequential surface reactions, provides accurate control of the thickness resulting in smooth and dense films.[9,10] Conformal coating can be achieved even in high aspect ratio and complex 3D structures.[11] Multicomponent films can be deposited by varying the sequence of different precursor pulses. The selection of suitable precursors for the rare earths is quite limited, but β-diketonate type precursors and ozone have been utilized to deposit most rare earth oxides.[12] The development of new volatile precursors is an important branch in the field of thin film technology, and new potential precursors containing direct metal-to-carbon bond (*e.g.* cyclopentadienyls) and nitrogen-bonded ligands (amides, amidinates and guanidinates) are being increasingly studied.[13,14]

The purpose of this thesis was to examine atomic layer deposition of high quality ternary rare earth oxide (*i.e.* mixed oxide of two different rare earth elements RERE´O_3) thin films and their properties in view of their potential use as high-κ dielectrics for MOSFETs. As background, a brief discussion of the high-κ problem and some requirements for the future high-κ materials are presented. Also some issues related to the search of suitable gate insulator materials for Ga-based compound semiconductor MOSFETs and the role of rare earth oxides in this task are discussed. Recent literature concerning the ALD processes of rare earth oxides as well as depositions of ternary rare earth oxide thin films is reviewed.

In the experimental part of the thesis atomic layer deposition of $RE^{I}Sc^{III}O_3$, $La^{III}Lu^{IV}O_3$ and $Er_xGa_{2-x}O_3$ thin films was studied. The emphasis was on trivalent rare earth oxides, and therefore *e.g.* CeO_2 was omitted. New deposition processes were developed by utilizing different precursor systems, including novel cyclopentadienyl and amidinate metal precursors. Properties essential for the high-κ dielectrics (*i.e.* impurity concentrations, crystallization behaviour and electrical characteristics) were analyzed.

2. MOSFET and the high-κ problem

Basic principles behind the metal-oxide-semiconductor field-effect transistor or MOSFET were first patented as early as 1928,[15] but the first operating device with thermally grown SiO_2 as gate oxide was fabricated thirty years later in 1959 and a patent filed in 1960.[16] For decades the basic structure of the MOSFET has not significantly changed, only the dimensions have decreased. There are several reasons for scaling down MOSFETs. The obvious and most important reason is the higher packing density of devices resulting in more functionality in a given area. The production costs for a semiconductor wafer are relatively fixed, and therefore increasing the number of chips per wafer directly reduces the price per chip. Smaller dimensions of the transistor also mean faster switching and faster operation of the device. At 1965 Gordon E. Moore published his famous prediction stating that the number of components on a single silicon chip would double every year.[17] This prediction, according to Moore's own words, was meant to be just an educated guess for the next ten years, and it was based on pure extrapolation from experiences gained during the past few years. Later in 1975, Moore modified his prediction saying that the doubling will happen every two years.[18] To this date, the prediction known as Moore's law has been fulfilled. But now the semiconductor industry has reached the limit where MOSFET cannot be made any smaller while still remaining functional. We are literally running out of atoms, as a crucial part of the MOSFET, *viz*. the gate oxide, traditionally made of SiO_2, cannot be made any thinner without losing its excellent insulating properties. Leakage current through the gate oxide causes components to run too hot and consume too much power which ultimately destroys the transistor operation.

2.1 Basic structure and operation of the MOSFET

The metal-oxide-semiconductor (MOS) structure may be described as a simple planar capacitor, with one of the electrode plates replaced by a semiconductor. When a positive voltage is applied between the gate and the p-type silicon body, major charge carriers, in this case holes are repelled away from the zone near the gate oxide interface and a carrier-free depletion layer of immobile, negatively charged acceptor ions is created. Further increase in the gate voltage causes a high concentration of minority charge carriers (*viz.* electrons) to appear and an inversion layer is formed at the oxide-semiconductor interface.

In MOSFET (Figure 1) two additional terminals, *viz.* source and drain are added to the basic MOS structure. If the body is p-type silicon, drain and source are identical, heavily n-doped regions. When a positive gate voltage is applied and the inversion layer is formed, an n-channel of enhanced electrical conductivity is created between the source and the drain, and current (*i.e.* drain current or drive current, I_D) can flow through the device. The number of charge carriers in the channel and therefore the current can be modulated by the gate voltage. The minimum voltage needed to create the inversion layer is called threshold voltage V_{th}.

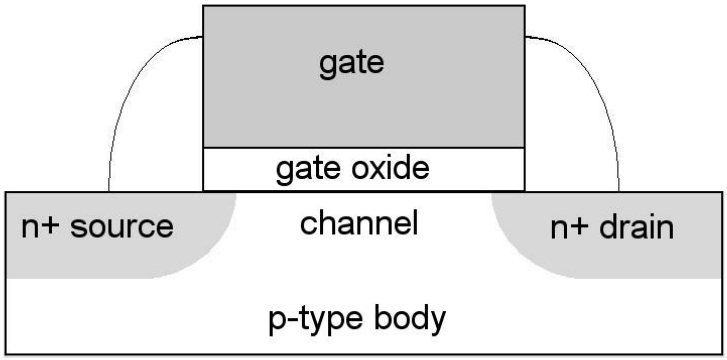

Figure 1. A Schematic showing MOSFET structure.

Applying the planar capacitor model for MOSFET, the capacitance C of the MOSFET is described by the equation

$$C = \kappa\varepsilon_0 \frac{A}{t} \tag{1}$$

and therefore the capacitance density $C_{d,\,inv}$ (at inversion) is described as

$$C_{d,inv} = \frac{C}{A} = \frac{\kappa\varepsilon_0}{t} \tag{2}$$

where A = capacitor area, κ = dielectric constant of the insulator material, ε_0 = permittivity of free space and t = thickness of the insulator layer.

Performance of a MOSFET is generally evaluated in terms of the drain current I_D at the saturation condition (*i.e.* $V_D \geq V_G$-V_{th}, V_D and V_G being the voltages applied to the transistor drain and gate,

respectively) and the simplest form of the saturation current for a long-channel device may be expressed as

$$I_{D,sat} = \frac{W}{L} \mu_{eff} C_{d,inv} \frac{(V_G - V_{th})^2}{2} \quad (3)$$

where W = channel width, L = channel length, μ_{eff} = effective channel carrier mobility, V_G = gate voltage and V_{th} = threshold voltage.

Increasing the term (V_G-V_{th}) is limited due to several reliability issues. Therefore, in order to increase the MOSFET drain current, the capacitance density $C_{d,inv}$ of the gate oxide has to be increased or the channel length L decreased. According to Eq. 2, increase in $C_{d,inv}$ is achieved by decreasing the insulator thickness t or by using material with higher κ. In 2002, Intel announced their 90 nm logic technology node with SiO_2 gate oxide thickness of only 1.2 nm,[19] which corresponds to *ca*. 5 atomic layers. This is already below the tunneling thickness, and devices with SiO_2 gate oxide this thin can only be operational when the gate length is reduced to *ca*. 0.1 μm or below.[20] However, with the gate oxide this thin, the leakage current is at the limit of being too high, causing components to run too hot and consume too much power. This is a major problem especially in portable devices.

When the SiO_2 gate oxide is replaced by a material with higher κ, the performance of the other high-κ material may be compared to that of SiO_2 in terms of equivalent oxide thickness (EOT), which indicates how thick a silicon oxide film would need to be in order to produce the same effect as the high-κ material being used. EOT is described by the equation

$$EOT = \frac{k_{SiO_2} t_{high-\kappa}}{\kappa_{high-\kappa}} \quad (4)$$

where κ_{SiO2} = dielectric constant of SiO_2 (= 3.9), $\kappa_{high-\kappa}$ = dielectric constant of the high-κ material and $t_{high-\kappa}$ = physical thickness of the high-κ layer. If an interfacial SiO_2 layer has formed between the Si substrate and the high-κ layer, the EOT for the whole gate oxide stack can be described as follows:

$$EOT = t_{SiO_2} + \frac{k_{SiO_2} t_{high-\kappa}}{\kappa_{high-\kappa}} \quad (5)$$

Extraction of EOT requires fitting of the capacitance–voltage (*C–V*) characteristics of the MOS structure, taking into account quantum confinement effects in the accumulation and inversion layers, as well as eventual poly-Si depletion effects. Therefore in many cases more practical quantity to compare different gate dielectrics is the capacitance equivalent thickness (CET), defined as

$$CET = \frac{\varepsilon_0 \kappa_{SiO_2}}{C_{\max}} \quad (6)$$

where C_{max} = the capacitance (per unit area) of the MOS structure measured at accumulation. The extraction of CET does not require fitting of the *C–V* data, but depends on the chosen gate bias.[21]

2.2 New high-κ materials on silicon

Until recently, the Si-SiO_2 system has been an ideal system from electrical, material and processing points of view. Replacement of SiO_2 by a new high-κ material brings many challenges to the traditional MOSFET manufacturing. In addition of finding a material, which fulfills the high standards of electrical properties set by this almost perfect insulator, it also has to be compatible with other materials and the existing CMOS (Complementary Metal Oxide Semiconductor) process. The electrical properties required include obviously high dielectric constant, but also large band gap and offsets to silicon conduction and valence bands as well as low leakage current. Large band offsets produce a potential barrier and therefore inhibit Schottky emission of electrons and holes. Other requirements include *e.g.* high interface quality, low density of interface and bulk states, and chemical stability with respect to both silicon and the gate material.[22] Either amorphous or high quality single crystal structure is required to minimize the leakage current or diffusion paths. Some of the most important requirements are listed in Table 1.

Table 1. Electrical properties of SiO_2 and requirements for replacing high-κ materials.[22,23]

	SiO_2	**high-κ**
Dielectric constant	3.9	12-30
Band gap	9 eV	> 5 eV
Valence band offset	4.8 eV	> 1 eV
Conduction band offset	3.1 eV	> 1 eV
Crystallization temperature	> 1000°C	> 1000°C
Interface density of states	(low)	$< 10^{11}$ cm^{-1} eV^{-1}

The dielectric constant should be in the range of 12-30, since higher κ may cause undesirable large fringing fields at the source and drain electrodes.[23] The band gap is a fundamental property of the material. Generally, increasing dielectric constant leads to narrower band gap, and therefore also lower conduction and valence band offsets in contact with silicon. For most high-κ oxides the conduction band offset is smaller than the valence band offset.[24] In Figure 2 band offsets of some high-κ candidates on silicon are presented.[25]

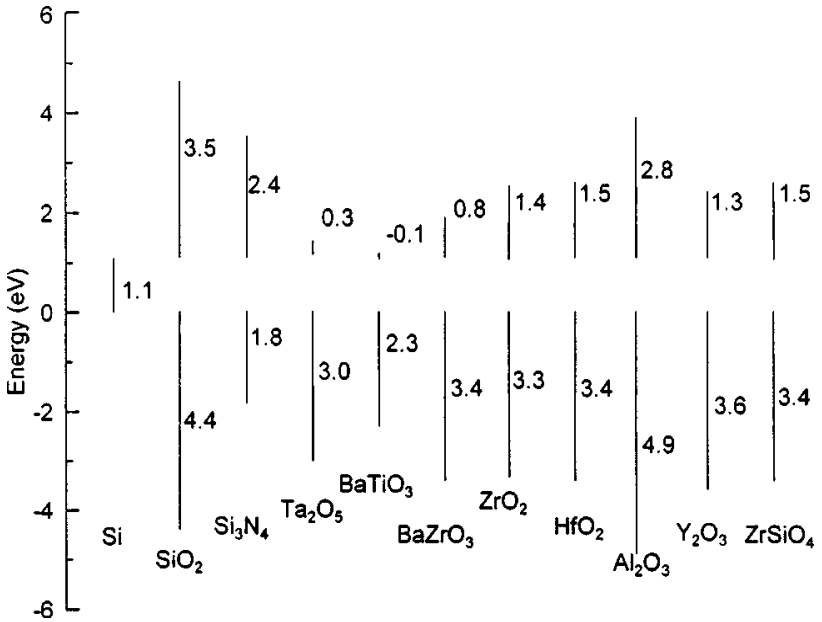

Figure 2. Calculated conduction band (upper row) and valence band (lower row) offsets of various materials on Si.[25]

Stability in contact with silicon and gate material is vital, even at high temperatures. The CMOS fabrication process includes thermal process steps up to 1000°C. Formation of a low-κ interfacial

layer between silicon and the gate oxide reduces the overall capacitance density of the gate oxide stack and therefore reduces also the MOSFET performance. The gate oxide should remain amorphous through the high temperature process steps since crystallization produces grain boundaries, creating diffusion paths for unwanted impurities and charge carriers. Until recently, the "metal" gate in MOSFET has actually been made of heavily doped polycrystalline silicon, *viz.* poly-Si, but it is not compatible with new high-κ oxides and causes channel mobility degradation due to Coulombic and phonon scattering. Therefore a mid-gap TiN metal gate has been introduced.[26] The gate oxide should provide a high-quality electrical interface, giving high carrier mobility in the channel and low defect density with low trapped charge and small gate threshold voltages.

It appears that hafnium oxide based materials, such as HfO_2,[27,28] $HfSi_xO_y$,[29] HfO_xN_y,[30] and $HfSi_xO_yN_z$[31,32] currently emerge as leading candidates. Pure HfO_2 has the highest dielectric constant ($\kappa \approx 20$-25), but it crystallizes at relatively low temperatures. For example, atomic layer deposition of HfO_2 at 350°C yields polycrystalline films.[33] Addition of Si and/or N increases the crystallization temperature,[30] but also reduces the dielectric constant. Of these materials only $HfSi_xO_yN_y$ remains amorphous after annealing at 1000°C, but it has a dielectric constant of only 14.[31] Incorporation of lanthanum into HfO_2 film has been proposed to increase the crystallization temperature with promising results.[34] The crystallization temperature of the films increased from 500°C up to 950°C with increasing La concentration while κ remained constant at 16.6-16.7. The first generation of microprocessors with a high-κ dielectric gate oxide manufactured since 2007 relies on hafnium oxide based gate insulator.[1,35] However, the trade-off between the crystallization temperature and the dielectric constant restricts the usage of hafnium oxide based materials, and for the next generation so called "higher-κ" applications new materials must be sought.

2.3 Rare earth oxides as high-κ dielectrics

Rare earth oxides have recently gained interest as possible high-κ oxides. Earliest studies focused on binary oxides, particularly La_2O_3, Gd_2O_3 and Y_2O_3.[22] By various physical vapor phase deposition methods Y_2O_3 films with a dielectric constant as high as 17-18 have been processed.[36,37] However, when chemical vapor deposition methods such as ALD[38] is applied, the dielectric constant of 10 is reported for Y_2O_3. Comparative study of lanthanoid oxides Ln_2O_3 grown by ALD provided κ in range of 8.4-11.1.[12] RE_2O_3 oxides have sufficiently large band gap (*ca.* 6 eV) and band offsets with silicon (valence and conduction band offsets *ca.* 2-3 eV) to be utilized as gate

oxides.[39] However, binary RE_2O_3 oxides easily crystallize which reduces the leakage current density. Incorporation of *e.g.* scandium into another RE_2O_3 increases both the dielectric constant and the crystallization temperature. For the most studied candidates, *viz.* $LaScO_3$,[III] $GdScO_3$[4,II] and $DyScO_3$,[III,5-7] dielectric constants $\kappa > 20$ and crystallization temperatures 900°C-1000°C have been reported. The band gaps and the band offsets (Table 2) also fulfill the requirements listed in Table 1.

Table 2. Band gaps and band offsets of interfaces between Si and some ternary rare earth oxides. The oxide films were deposited by pulsed laser deposition.[40]

	Band gap E_g (eV)	**Band offsets**	
		Conduction band ΔE_c (eV)	**Valence band ΔE_v (eV)**
$LaScO_3$	5.7 ± 0.1	2.0 ± 0.1	2.5 ± 0.1
$GdScO_3$	5.6 ± 0.1	2.0 ± 0.1	2.5 ± 0.1
$DyScO_3$	5.7 ± 0.1	2.0 ± 0.1	2.5 ± 0.1

2.4 GaAs-based electronics

Although silicon is by far the most common semiconductor material, GaAs and other III-V compound semiconductors have some properties, such as excellent optoelectronic properties and high electron mobility, which make them more suitable than silicon for some specific applications. Better performance comes with the price of more complicated processing and higher cost, therefore III-V semiconductors are only used in applications where the performance is more important than the cost. The main obstacle to GaAs-based MOSFET devices is the lack of high-quality, thermodynamically stable insulators on GaAs that could match the device criteria as SiO_2 on Si. Unlike silicon, GaAs does not have stable native oxide which could be used as a gate oxide in GaAs MOSFETs. The major challenge is to create a high quality interface with low density of interface states (D_{it}) between the GaAs and the insulator. Most early studies have concentrated on oxidizing the GaAs surface by various gas and liquid phase methods.[41,42] However, the quality of these oxide layers was not as high as needed, and therefore the next approach to solve the problem was to deposit pure Ga_2O_3 thin film onto GaAs. In order to slow down the deposition process and prevent splattering of Ga_2O_3 due to rapid sublimation, a $Gd_3Ga_5O_{12}$ garnet (GGG) was used as target in electron beam evaporation of Ga_2O_3 thin films.[43] Gd_2O_3 has much higher evaporation temperature (~ 4000 K) than Ga_2O_3 (~ 2000 K), and it was expected that high quality Ga_2O_3 film could be produced by this method. It turned out that the small amount of Gd found as an impurity in the films was a key to high quality films with low D_{it}. The effect of Gd was investigated in more detail

and a series of $(Ga_2O_3)_{1-x}(Gd_2O_3)_x$ (x=0-1.0) films were deposited by electron beam evaporation.[44] It was concluded that the lowest D_{it} and leakage current density were achieved when x was in the range 14-20 %. However, the fundamental reason for this behaviour and the role of Gd are not clear. It was suggested that as an electropositive element Gd stabilizes the Ga +3 oxidation state therefore preventing the formation of gallium suboxides (GaO and Ga_2O) and also minimizing the concentration of oxygen vacancies.[44] It was also suggested that other electropositive elements (rare earth and alkaline earth elements) would have similar beneficial effect on the properties of Ga_2O_3. Also rare earth oxides Gd_2O_3, $(Gd_xLa_{1-x})_2O_3$ and Gd-silicate have been deposited by physical vapor deposition methods on GaAs.[45,46] The first GaAs MOSFET with the gate oxide (Al_2O_3) deposited by ALD has also been fabricated.[47]

3. Atomic layer deposition method

The atomic layer deposition (ALD) method was developed in the 1970s by Suntola and Antson[48] to produce high-quality, large-area flat panel electroluminescence displays, but is nowadays studied for various applications.[10] ALD can be considered as an advanced version of the chemical vapor deposition (CVD) method and it relies on self-saturated surface-limited reactions of alternately introduced vaporized precursors. Precursor pulses are separated by inert gas purge in order to remove any excess precursor molecules and gaseous reaction by-products, leaving the growing film surface saturated by the previous precursor and ready to react with the next precursor. Due to the surface-controlled nature of the deposition, the film grows conformally regardless the shape of the substrate (planar, trenches, porous, *etc.*).[11] The thickness of the film can be controlled by simply adjusting the number of deposition cycles as demonstrated in Figure 3. Although the ALD method is generally employed in the deposition of binary films such as oxides, nitrides and sulfides, more complex films can also be deposited.[49] Varying the ratio of different precursor pulses the elemental composition of the film can be fine-tuned.

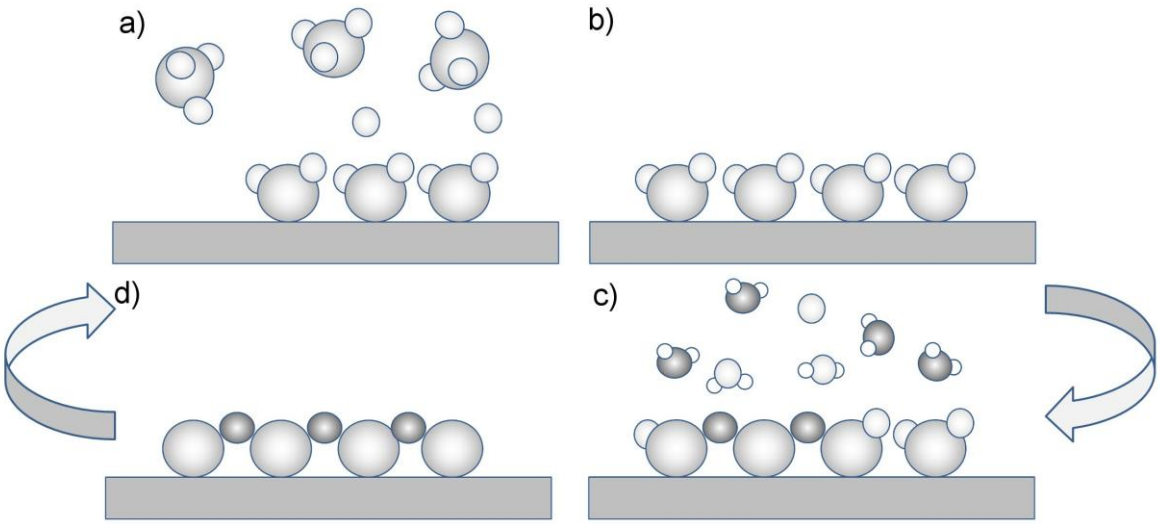

Figure 3. One ALD cycle consists of four separate steps. a) The substrate is exposed to precursor 1 molecules which adsorb ideally as a monolayer on the surface. b) The excess is removed by inert gas purging. c) The substrate is exposed to precursor 2 which reacts with the adsorbed precursor 1 to form a layer of the desired material. d) Finally the excess of precursor 2 and the reaction by-products are removed by purging. The cycle is repeated until the desired thickness of the film is obtained.

One drawback of the ALD method is the relatively slow deposition rate, but considering the extremely thin layers needed in microelectronic devices this is not a major concern. Another concern is the limited number of suitable precursors for some elements. This can be especially problematic when depositing multi-element thin films, since all the chosen precursors must provide surface-limited film growth at the same deposition temperature. The precursors must be chemically compatible and reactive, *viz.* each precursor must react with the surface as it is after the preceding precursor pulse and inert gas purge.

4. Rare earth oxide thin films

Rare earth oxide thin films have been deposited by both physical and chemical vapor phase methods. In this thesis the focus is on atomic layer deposition and therefore recent literature concerning ALD of RE_2O_3 thin films is briefly reviewed. Ternary rare earth oxides have mostly been deposited by physical vapor deposition methods and essential properties of those thin films is discussed.

4.1 Chemistry of the rare earth oxides

Despite the name, many of the rare earth elements are not rare at all in the earth's crust. The name originates from the history of their discovery. Due to their similarity in size and oxidation state, in nature the rare earth elements are found together, and for a long time it was very difficult to separate them. They are all electropositive reactive metals, the most important oxidation state is +3, and due to their large size and oxidation state the bonding is predominantly ionic in character.[50] Especially the larger rare earths are basic in their chemical behaviour. Binary RE_2O_3 can adopt different structures, a hexagonal A-type and a cubic C-type being the most common at low and moderately elevated temperatures.[51] Larger RE oxides favor the A-type structure while smaller RE oxides, including yttrium and scandium oxides prefer the C-type structure. When two rare earth oxides are combined, the size difference between the RE^{3+} cations determines which crystal structure the ternary oxide adopts. If the cations are similar in size and the preferred crystal structure of the oxides is the same, a solid solution is easily formed. However, when the size difference between the two REs increases, an orthorhombic perovskite phase can be formed. In the bulk form, ternary $REScO_3$ with the perovskite structure have been synthesized at ambient pressure when RE=La, Pr, Nd, Sm, Eu, Gd, Tb, Dy and Ho.[52] Smaller rare earth elements do not form perovskites under ambient conditions, but high-pressure syntheses of $YScO_3$, $HoScO_3$, $ErScO_3$ and $TmScO_3$ have been reported.[53] The deposition method and the substrate affect many of the thin film properties, and materials may behave quite differently in thin film form. Low-energy interfaces facilitate the formation of otherwise unstable compounds or structures and even the smallest RE lutetium forms the ternary $LuScO_3$ perovskite phase when deposited onto $NdGaO_3$(110) and $DyScO_3$(110) substrates.[54] When the crystallization behaviour of $REScO_3$ thin films deposited by pulsed laser deposition (PLD) on $LaAlO_3$ substrates was studied, a correlation between the atomic number of

RE and the crystallization temperature was found.[55] $REScO_3$ perovskite phase was observed when RE=La-Ho, but $TmScO_3$, $YbScO_3$ and $LuScO_3$ did not form the perovskite phase at the temperature range examined which was up to 800°C.

4.2 Atomic layer deposition of binary rare earth oxides

4.2.1 RE metal precursors

As discussed in chapter 3, one limitation of the ALD method for many elements is the lack of suitable precursors. In general, the ALD precursor must be volatile, thermally stable at the deposition temperature and react readily with the surface and the other precursor.[56] Although oxides of all naturally occurring rare earths have been deposited by ALD, the range of available precursors is quite limited. Many transition metal oxides (*e.g.* HfO_2[27], ZrO_2[57] and TiO_2[58]) have been deposited by ALD utilizing halides, but rare earth halides are not sufficiently volatile to be used as precursors. Instead, several volatile complexes with organic ligands provide the necessary properties. (Figure 4.)

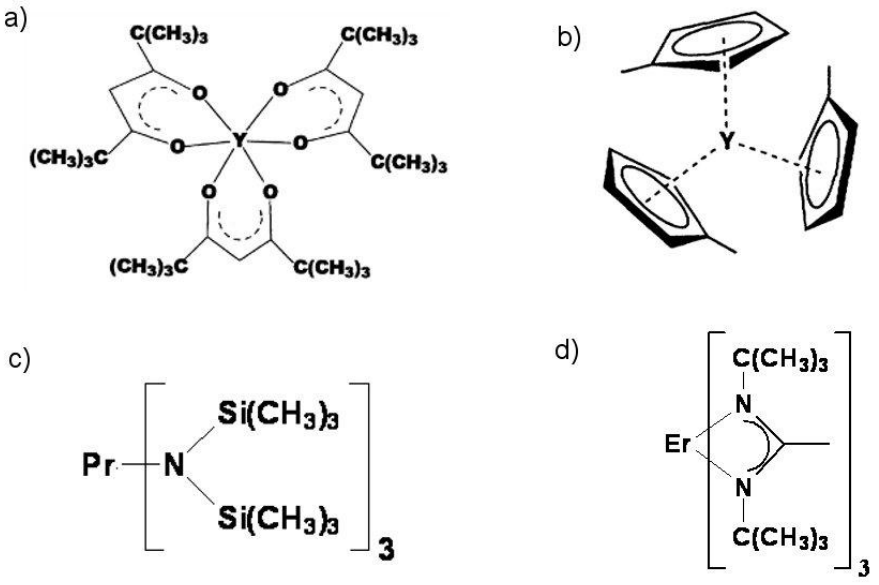

Figure 4. Typical volatile RE compound which can be utilized in ALD of rare earth oxides
a) β-diketonate $Y(thd)_3$, b) cyclopentadienyl compound $(CpMe)_3Y$, c) silylamide $Pr[N(SiMe_3)_2]_3$ and d) amidinate $Er(^tBu_2amd)_3$.

β-diketonates

Rare earth β-diketonates are the most popular and the most intensively investigated rare earth coordination compounds.[59] The first RE β-diketonates were prepared already at the end of the 19th century,[60] and since then they have been utilized in many different fields. RE β-diketonates were first used in ALD when electroluminescence ZnS films were doped with lanthanoids in the late 1980s.[61] The first RE oxides grown by ALD using thd-based (thd=2,2,6,6-tetramethyl-3,5-heptanedionato) precursors and ozone were Y_2O_3,[62] CeO_2[63] and La_2O_3.[64] Since these early reports almost all RE oxides have been successfully deposited by thd-based processes.[12,65-74]

The β-diketonates have two carbonyl groups separated by one carbon atom, thus they can act as bidentate chelating agents. The simplest β-diketonate is acetylacetone (Hacac), where the substituents on both carbonyl groups are methyl groups. In 2,2,6,6-tetramethyl-3,5-heptanedione (Hthd), these methyl groups are replaced by bulkier *tert*-butyl-groups. The neutral *tris*-complexes have three β-diketonate ligands for each RE^{3+} ion and the general formula is thus RE(β-diketonate)$_3$. Because the coordination sphere of especially the larger RE^{3+} ions is unsaturated in these six-coordinate complexes, the RE can expand its coordination sphere by oligomerization with bridging β-diketonate ligands. However, the oligomerization may reduce the volatility of the complex. In the RE thd-complexes, branched *tert*-butyl-groups provide steric protection, stabilize the complexes and increase their volatility, making them suitable precursors for ALD. Although especially the larger RE(thd)$_3$ crystallize as dimers[75], mass spectrometric studies of RE(thd)$_3$ have not revealed any dimers in the gas phase.[76] The main peak corresponds to $RE(thd)_2^+$, but the molecular RE(thd)$_3$ is also present. Another option to saturate the coordination sphere is by adduct formation with Lewis bases, such as 1,10-phenantroline or 2,2'-bipyridine.[66] This approach has been applied to coordinatively saturate and stabilize the otherwise unstable Ce^{3+} ion.[77] The chelate effect and REs' strong tendency to form oxygen-coordinated complexes make thd-compounds stable and unreactive towards mild oxidizers. Therefore aggressive oxidizers such as ozone are needed to break the RE-thd bond yielding RE oxide thin film. Although the deposition rate is slow due to the bulky ligands, the films deposited by the thd-process are generally of high quality and have only a few impurities, mainly carbon.

Cyclopentadienyl compounds

The first cyclopentadienyl (Cp) compounds of rare earths were synthetized by Wilkinson and Birmingham in 1954.[78] Air- and moisture sensitive rare earth Cp-complexes are highly reactive towards water which make them desirable metal precursors for ALD. Considering the ALD of gate oxides in particular, the fact that no aggressive oxygen source such as ozone is required is beneficial, since the oxidation of the silicon substrate and therefore the growth of interfacial SiO_2 layer can be minimized. Also the deposition rate is much higher compared to *e.g.* thd-processes. However, due to their higher reactivity special attention must be paid to the storage and handling of the precursors.

Simple *tris*-cyclopentadienyl complexes of the smaller rare earths, *viz.* Y and Sc, have been utilized in ALD, [38,65] resulting in smooth films with very little impurities. However, when the radius of the RE^{3+} cation increases, unsubstituted Cp ligands can no longer saturate the coordination sphere of the large central cation. Cp_3RE compounds of larger REs decompose upon heating destroying the self-limiting nature of the ALD growth. Larger, substituted ligands and/or adducts stabilize the complex, but even then the deposition of high quality film can be difficult. In his dissertation,[28] J. Niinistö reports that Cp_3La decomposes at its relatively high sublimation temperature (250°C) and therefore further deposition experiments were not continued. Bulkier $(CpMe)_3La$, $(CpMe4)_3La$ and $(Cp^iPr)_3La$ had better thermal stability and some uniform films were deposited, but only at very low temperatures, viz. 190°C. Even then the growth was not fully surface-limited, since longer precursor pulses resulted in higher growth rates. However, Scarel *et al.*[79] and Tsoutsou *et al.*[80] managed to deposit La_2O_3 films by ALD using unsubstituted Cp_3La and water at 260°C. The sublimation temperature of the Cp_3La precursor in these depositions was lower (185°C) than reported in Niinistö's dissertation (250°C), which may be the explanation why Scarel and Tsousou managed to utilize Cp_3La in ALD. Other details of the deposition process were not reported. Methyl-substituted cyclopentadienyl compounds have successfully been employed in deposition of Y_2O_3[38] and Er_2O_3.[81] Gd_2O_3 thin films of satisfactory quality were deposited using $(CpCH_3)_3Gd$ and water as precursors even though $(CpCH_3)_3Gd$ showed signs of decomposition during the deposition.[73] Further increase in the substituent size stabilizes the Cp-compounds; Kim *et al.* have managed to deposit La_2O_3 by electron cyclotron resonance atomic layer deposition (ECR-ALD) technique with tris(isopropyl-cyclopentadienyl)lanthanum [$(iPrCp)_3La$] as a lanthanum precursor and O_2 plasma as the oxygen source.[82] Truly self-limiting growth behaviour was observed when the deposition temperature exceeded 300°C.

Amides

Rare earth complexes with nitrogen-coordinated ligands could be interesting precursors for ALD, since they are presumably more reactive towards water compared to *e.g.* β-diketonates. Simple rare earth alkylamides [$RE(NR_2)_3$] are too unstable and involatile to be utilized as precursors in ALD,[83] but substituting the ligand with bulky trimethylsilyl-group produces relatively stable and volatile monomeric rare earth *tris*-silylamides $RE[N(SiMe_3)_2]_3$[84] which have been utilized in ALD of La_2O_3,[85-90] PrOx[91] and Gd_2O_3.[83,92] However, the resulting oxide films contained considerable amount of impurities (mainly Si and H) and crystallized upon annealing as mixed silicate films. For PrOx[91] and Gd_2O_3[83,92] the growth rate increased with increasing precursor pulse length indicating the growth was not fully surface saturated. Kukli *et al.* reported very peculiar growth for the La_2O_3 films where the growth rate decreased with increasing metal precursor pulse length, which is very untypical for ALD.[89]

Amidinates and guanidinates

Rare earth amidinates and guanidinates comprise a relatively new class of complexes containing N-chelating ligands as they were discovered less than 20 years ago.[13] At first, no practical uses were envisaged, but once their potential in homogeneous catalysis in 2002 was discovered,[93] activity in this field increased enormously. The high volatility, thermal stability, and high and properly self-limited reactivity with water vapor make these compounds excellent precursors for ALD. The first RE oxide thin films deposited by ALD using amidinate precursor were La_2O_3.[94,95] Also Sc_2O_3[96] and Y_2O_3[97] thin films have been deposited by $RE(^{i}Pr_2amd)_3$ precursors together with water, but surprisingly no reaction occurred between amidinato complex $Er(^{t}Bu_2amd)_3$ and water.[98] Instead, ozone was utilized as an oxygen source, but the growth was not fully surface saturated. Amidinate anions (general formula $[RC(NR')_2]^-$) are the nitrogen analogues of the carboxylates. All three substituents at the heteroallylic N-C-N unit can be varied in order to meet a large range of steric requirements. Closely related guanidinate ions contain a tertiary amino group at the central carbon atom of the N-C-N unit.[14] Like the β-diketonates, acting as bidentate chelating agents amidinates and guanidinates are expected to enhance the thermal and chemical stability of the resulting metal complexes and thus make them suitable precursors for ALD. By selecting appropriate substituents the steric and electronic properties of the ligands can be fine-tuned and *e.g.* volatility of the

resulting complex increased. Guanidinate precursor has recently been utilized in ALD of Gd_2O_3 thin films.[14, 99]

4.2.2 RE_2O_3 films by ALD

In Table 3 some representative examples of ALD of binary RE_2O_3 thin films are presented. Due to the increasing number of publications and somewhat incoherent practices in reporting the results the table is not fully comprehensive, but it should give an overview of the ALD processes applied.

Table 3. Typical examples of binary RE_2O_3 thin films grown by ALD.

RE_2O_3	Metal precursor	Oxygen source	Deposition temperature (°C)	Growth rate (Å/cycle)	Ref.
Sc_2O_3	$Sc(thd)_3$	O_3	335-375	0.13	[65]
	$Sc(thd)_3$	$O_3 + H_2O_2$	375	0.14	[65]
	Cp_3Sc	H_2O	250-350	0.75	[65]
	$Sc(^iPr_2amd)_3$	H_2O	290	0.3	[96]
Y_2O_3	$Y(thd)_3$	O_3	250-350	0.23	[66, 67]
	$Y(thd)_3$	O_2 plasma	200-300	0.3-0.5	[69-71]
	$Y(thd)_3$(bipy)	O_3	250-350	0.23	[66]
	$Y(thd)_3$(phen)	O_3	250-350	0.22	[66]
	Cp_3Y	H_2O	300	1.62	[38]
	$(CpMe)_3Y$	H_2O	200-400	1.2-1.3	[38]
	$Y(^iPr_2amd)_3$	H_2O	150-280	0.8	[97]
La_2O_3	$La(thd)_3$	O_3	225-275	0.36	[68, 100]
	Cp_3La	H_2O	260*	(not reported)	[79, 80]
	$(CpEt)_3La$	O_2 plasma	> 300	0.2	[101]
	$(Cp^iPr)_3La$	O_2 plasma	300	0.6	[82, 102]
	$La[N(SiMe_3)_2]_3$	H_2O	225-275	0.3-0.5	[85-90]
	$La(^iPr\text{-}amd)_3$	H_2O	300	0.9	[94, 95]
PrO_x	$Pr(thd)_3$	O_3	200*	0.52-0.71	[74]
	$(Cp^iPr)_3Pr$	H_2O	175*	1.6	[28]
	$Pr[N(SiMe_3)_2]_3$	H_2O	200-300*	0.15-0.3	[91, 92]
Nd_2O_3	$Nd(thd)_3$	O_3	275-325	0.44-0.45	[12,72]
Sm_2O_3	$Sm(thd)_3$	O_3	300	0.36	[12]
Eu_2O_3	$Eu(thd)_3$	O_3	300	0.32	[12]
Gd_2O_3	$Gd(thd)_3$	O_3	250-300	0.30-0.31	[12, 73]
	$(CpMe)_3Gd$	H_2O	250-300*	*ca.* 2.0-3.0	[73]
	$Gd[N(SiMe_3)_2]_3$	H_2O	200-250*	*ca.* 0.5-2.2	[92]
	$Gd[(^iPrN)_2CNMe]_3$	H_2O	175-275	1.1	[14, 99]
Dy_2O_3	$Dy(thd)_3$	O_3	300	0.31	[12]
Ho_2O_3	$Ho(thd)_3$	O_3	300	0.25	[12]
Er_2O_3	$Er(thd)_3$	O_3	250-375	0.24-0.25	[12, 103]
	$Er(thd)_3$	O_2 plasma	300	0.3-0.5	[69, 70]
	$(CpMe)_3Er$	H_2O	250-350	1.5	[81]
	$Er(^tBu_2amd)_3$	O_3	225-300*	0.37-0.55	[98]
Tm_2O_3	$Tm(thd)_3$	O_3	300	0.22	[12]
Yb_2O_3	$Yb(thd)_3$	O_3	300-350	0.15	[104]
	Cp_3Yb	H_2O	360*	0.2-0.36	[105]
	Cp_3Yb	O_3	360*	0.11-0.24	[105]
Lu_2O_3	$\{[Cp(SiMe_3)]_2LuCl\}_2$	H_2O	360*	0.26, 0.9-1.4	[105, 106]

*surface saturated ALD growth not observed or not fully studied

4.3 Ternary RE-oxide thin films

Ternary rare earth oxide thin films have mostly been deposited by physical vapor deposition methods such as pulsed laser deposition (PLD)[2,3,107] and molecular beam deposition (MBD),[108-111] but a few reports of MOCVD[112,113] and ALD[I-IV,114] have been published. In Table 4 representative examples of ternary RE-oxides depositions are presented and the some properties of the films summarized. Although the listing is far from complete due to vast number of publications in this field, it should give an overall picture of deposition methods applied and some typical properties of the films. The emphasis is on amorphous high-κ thin films deposited on silicon.

Table 4. Examples of amorphous high-κ ternary rare earth oxides deposited on silicon.

Thin film	**Deposition method**	**κ**	**Crystallization temperature (°C)**	**Ref.**
$YScO_3$	ALD	14-16	800-1000	[I]
$LaScO_3$	ALD	16	800	[III, 114]
	PLD	22	800	[2, 3]
	MBD	17 (as-dep.) 28-33 (annealed)	800	[108-111]
$SmScO_3$	PLD	29	900	[107]
$GdScO_3$	ALD	22	900	[II,115]
	MOCVD	(not reported)	1100	[112]
	PLD	22	1100	[2, 3]
	EBE	23	1100	[4]
$TbScO_3$	EBE	26	> 1100	[116]
$DyScO_3$	ALD	24	900	[III]
	MOCVD	20-23	1100	[5-6, 113]
	PLD	22	1100	[2, 3]
$ErScO_3$	ALD	18	600	[III]
$LuScO_3$	ALD	11	300	[III]
$LaLuO_3$	ALD	30	900	[IV, 114, 117]
	MOCVD	(not reported)	1000	[112]
	PLD	17 (as-dep.) 32 (annealed)	800-1100	[111, 118]
	MBD	30	800	[117]

Typical issues and problems encountered are interdiffusion of the substrate and the thin film material resulting in unwanted reactions and formation of interfacial layer degrading the film properties. It has been shown that MOCVD-deposited $DyScO_3$ films react with the underlying SiO_2 layer at temperatures *ca.* 800°C and thereupon an amorphous silicate layer is formed.[113,119] The same phenomenon was also detected with $LaScO_3$ films deposited by MBD.[110] The extent of Si diffusion seems to depend on many factors, *e.g.* annealing temperature, atmosphere and the quality of the SiO_2 layer between the silicon substrate and the $REScO_3$ film. Also the thickness of the original $REScO_3$ layer plays a significant role. At 1000°C, a thin (*ca.* 4 nm) $DyScO_3$ film was completely transformed into amorphous $Dy_xSc_ySi_zO_\delta$ layer,[113] but in the case of an originally thicker (*ca.* 12 nm) $DyScO_3$ film, a polycrystalline $DyScO_3$ layer was formed on top of an amorphous silicon rich layer.[119] When the reaction between binary RE_2O_3 films and silicon substrates was investigated after thermal annealing, it was concluded that the larger the ionic radius of the RE^{3+} is, the more easily Si diffuses into the RE_2O_3 film.[120]

5. Experimental

This section briefly describes depositions and analyses of the thin films. A more detailed description can be found in publications I-V. In addition to the processes described in publications, depositions of $HoScO_3$ and some additional depositions of $REScO_3$ and $LaLuO_3$ thin films at higher temperature are discussed.

5.1 Thin film depositions

All ALD depositions were carried out in a commercial flow-type hot-wall ALD-rector (F-120 by ASM Microchemistry Ltd.). Nitrogen (> 99.999%) used as carrier and purge gas was generated in Schmidlin UHPN 3000 N_2 generator. The pressure in the reactor during the depositions was *ca.* 2-3 mbar. Most depositions utilizing β-diketonate metal precursors were carried out at 300°C, but for $YScO_3$, $HoScO_3$ and $Er_xGa_{2-x}O_3$ higher deposition temperatures were used. Deposition of $DyScO_3$ and $LaLuO_3$ films was studied also at slightly higher temperature, *viz.* 350°C. With cyclopentadienyl or amidinate metal precursors deposition temperatures 250°C ($Er_xGa_{2-x}O_3$) and 300°C ($YScO_3$) were applied.

$RE(thd)_3$ precursors were synthesized in the laboratory by method originally described by Eisentraut and Sievers[121] and purified by sublimation under reduced pressure. All other precursors were obtained from elsewhere (details in original publications I-V.) Due to their highly air and moisture sensitive nature, cyclopentadienyl- and amidinate-precursors (*viz.* $(CpMe)_3Y$, $(CpMe)_3Er$, Cp_3Sc and $(NMe_2)_6Ga_2$) were stored and handled under argon in a glove-box. All precursors were solid and they were sublimed from open glass crucibles inside the reactor. Air sensitive precursors were loaded into the crucibles in a glove box and sealed inside a glass tube which then could be transferred into the reactor. Ozone produced from 99.999% O_2 in Fischer Model 502 ozone generator was used as oxygen source with the β-diketonate precursors $RE(thd)_3$ and $Ga(acac)_3$. Water was used with the more reactive cyclopentadienyl and amidinate precursors and it was evaporated from an external container kept at room temperature.

Films were deposited onto two 5 cm x 5 cm p-type Si(100) substrates (Okmetic Ltd., Vantaa, Finland). Substrates were placed one after the other along the gas flow direction. Soda lime glass

substrates of similar size were used on the backside to prevent film growth on the back of silicon. Silicon substrates were mostly used as received, but in case of $REScO_3$ (RE=La, Gd, Dy, Er or Lu) and $LaLuO_3$ films substrates for the samples intended for electrical characterization were dipped into 2 % HF solution prior to the depositions to remove the native oxide layer. Glass substrates were ultrasonically cleaned in ethanol and water before use. Only in the case of $YScO_3$ also films deposited on glass were analyzed.

All ternary deposition processes were based on previously well documented binary deposition processes with already optimized parameters (*i.e.* deposition and precursor sublimation temperatures, precursor pulse and purge lengths *etc.*). Ternary processes were established by combining two binary processes without a detailed optimization of parameters. In some thd-depositions slightly longer precursor pulses (typically 1.5 s for metal precursors and 2.0 s for ozone) were used to ensure surface saturation and high quality of films over the entire substrate area, but this did not have any effect on the deposition rate of the films.

Some additional depositions not described in original publications I-V were also carried out. These include deposition of $HoScO_3$ thin films and also additional deposition of $DyScO_3$ and $LaLuO_3$ thin films at 350°C using thd-precursors and ozone. For $HoScO_3$ depositions very similar conditions except the deposition temperature (350°C) were applied as described in publication III for other $REScO_3$, including precursor pulse and purge lengths. Sublimation temperature of $Ho(thd)_3$ was 130°C. For $DyScO_3$ and $LaLuO_3$ deposition parameters apart from the deposition temperature were the same as described in publications III and V, respectively. Table 5. summarizes all thin film materials, precursors and deposition temperatures included in this thesis.

Table 5. Thin film depositions included in this thesis.

Film material	Metal precursors	Oxygen source	T_{dep} (°C)	Ref.
$REScO_3$ thin films				
$YScO_3$	$Y(thd)_3$, $Sc(thd)_3$	O_3	335, 350	[I]
	$(CpMe)_3Y$, Cp_3Sc	H_2O	300	[I]
$LaScO_3$	$La(thd)_3$, $Sc(thd)_3$	O_3	300	[III]
$GdScO_3$	$Gd(thd)_3$, $Sc(thd)_3$	O_3	300	[II]
$DyScO_3$	$Dy(thd)_3$, $Sc(thd)_3$	O_3	300, 350	[III, ch. 6.1]
$HoScO_3$	$Ho(thd)_3$, $Sc(thd)_3$	O_3	350	[ch. 6.1]
$ErScO_3$	$Er(thd)_3$, $Sc(thd)_3$	O_3	300	[III]
$LuScO_3$	$Lu(thd)_3$, $Sc(thd)_3$	O_3	300	[III]
Other ternary thin films				
$LaLuO_3$	$La(thd)_3$, $Lu(thd)_3$	O_3	300, 350	[IV, ch. 6.3]
$ErGaO_3$	$Er(thd)_3$, $Ga(acac)_3$	O_3	350	[V]
	$(CpMe)_3Er$, $(NMe_2)_6Ga_2$	H_2O	250	[V]

5.2 Film characterization

In case of $REScO_3$ and $LaLuO_3$, it was attempted to grow films with composition as close as possible to the stoichiometric structure. During the optimization of the film stoichiometry, the metal ratio was measured by X-ray fluorescence spectrometry (XRF, Philips PW 1480 WDS spectrometer) using Rh excitation. The data were analyzed with the UniQuant 4.34 program (Omega Data Systems, Netherlands), which is based on fundamental parameters and experimentally determined instrumental sensitivity factors.[122,123] XRF is a rapid and non-destructive method to analyze heavier elements (typically metals) and is therefore well suited for the preliminary examination of the metal ratio in ternary thin films. When a metal ratio close to the stoichiometric one (~1) was observed, a series of samples of different thicknesses (typically from 5 nm to *ca.* 100 nm) were deposited. Metal ratio in $REScO_3$ (RE=La, Gd, Dy, Er and Lu), $LaLuO_3$ and $Er_xGa_{2-x}O_3$ films was then verified by Rutherford backscattering spectrometry (RBS) at the Institute of Bio- and Nanosystems and Center of Nanoelectronic Systems for Information Technology, Research Center Jülich, Germany or at the Interuniversity Microelectronics Center, Belgium. RBS and other ion beam methods are especially suitable for compositional analysis of thin material layers.[124] No standards nor preliminary knowledge of the sample composition is required. RBS is based on probing backscattered ions when the sample is bombarded by typically 1.0-2.5 MeV He ions. It is

especially powerful method for detection of metals and other heavy elements and gives also information of the elemental depth profile.

Time-of-flight elastic recoil detection analysis (TOF-ERDA)[124] was utilized in analyzing the metal to oxygen ratio and possible light elements in the films. TOF-ERDA is an ion beam analysis method and relies on coincident detection of time-of-flight and energy of forward-scattering sample ions when the sample is bombarded by heavy incident ions. Unlike RBS and XRF, TOF-ERDA can detect even the lightest of elements including hydrogen. In case of $YScO_3$ and $HoScO_3$ films also the metal ratio RE:Sc was verified by TOF-ERDA. TOF-ERDA measurements were carried out at the Acceleration laboratory of the University of Helsinki and at the Interuniversity Microelectronics Center, Belgium. Fourier transform infrared spectroscopy (FTIR) was used for the speciation of carbon impurities in films. Rare earth oxide thin films deposited with carbon containing precursor and ozone often contain carbonate which can be easily recognized by its characteristic bands.[12,68] Samples were analyzed in a Nicolet Magna-750 infrared spectrometer.

The growth rates for films with thickness > 50 nm were calculated from thickness data determined by an optical fitting method described by Ylilammi and Ranta-aho.[125] In this method, theoretical spectra were fitted to reflectance spectra (190-1100 nm) measured in a Hitachi U-2000 double beam spectrophotometer. Thinner films (*ca.* 5-50 nm) were analyzed by X-ray reflectometry (XRR) for thickness. Selected samples of $GdScO_3$ were also analyzed by transmission electron spectroscopy (TEM) to verify the film thickness and by spectroscopic ellipsometry (SE) for thickness variation. TEM, XRR and SE analyzes were carried out at the Institute of Bio- and Nanosystems and Center of Nanoelectronic Systems for Information Technology, Research Center Jülich, Germany.

Crystallinity of the films was analyzed by X-ray diffraction method using both a traditional (Philips MPD 1880) and a grazing incidence (Panalytical X'Pert Pro MDP) mode. Samples were analyzed before and after thermal annealing. Annealings were carried out in nitrogen atmosphere for 10 min at temperatures varying from 500°C to 1000°C using PEO 601 (ATV Technologie GmbH) rapid thermal annealing oven. $LaLuO_3$ films were also annealed under oxygen and after annealing examined by XRD. These analyses were carried out at the Institute of Bio- and Nanosystems and Center of Nanoelectronic Systems for Information Technology, Research Center Jülich, Germany. Surface morphology of $YScO_3$, $GdScO_3$ and $Er_xGa_{2-x}O_3$ films were analyzed by atomic force microscopy (AFM). Nanoscope III (Digital Instruments) was operated in tapping mode and scanning frequency of 1 Hz. Roughness values were calculated as root mean square (rms) values.

For $YScO_3$ and $Er_xGa_{2-x}O_3$ thin films Al/insulator/SiO_2/p-Si(100)/Al capacitor structures were constructed. The thickness of the dielectric layer was *ca.* 40-50 nm. The effective dielectric constant was calculated from the accumulation capacitance. For other films Pt/insulator/p-Si(100)/Al structure were constructed and films with varying thicknesses (typically from. *ca.* 5 nm to 20 nm, but for $DyScO_3$ and $LaLuO_3$ also thicker films) were analyzed. CET (capacitance equivalent thickness) values were plotted versus the physical film thickness and the dielectric constant was extracted from the slope of resulting straight line. Table 6 summarizes the analysis methods used in this thesis.

Table 6. Summary of the analysis methods applied and the information acquired.

Method	**Information obtained**	**Publication**
UV/VIS spectrophotometry	Film thickness (> 50 nm), growth rate	I-V
XRR	Film thickness (5 - 50 nm), growth rate	I-V
XRF	Metal ratio	I-III, V
RBS	Metal ratio	II-V
TOF-ERDA	M:O ratio, impurities, metal ratio	I-III, V
FTIR spectroscopy	Detection of carbonate	I, III
XRD, GIXRD	Crystallinity	I-V
AFM	Surface morphology	I-II, IV-V
TEM	Structure, thickness, detection of the interface layer	II, IV
Spectroscopic ellipsometry	Thickness variation	II
XPS	M:O ratio	IV
C-V measurement	CET, κ, V_{Fb}, hysteresis	I-V
I-V measurement	Leakage current density	I-V

6. Results and discussions

This chapter summarizes the results of the thin film depositions. First the depositions and properties of the $REScO_3$ thin films grown by the thd-process are discussed and some previously unpublished results are included. $YScO_3$ thin film depositions utilizing cyclopentadienyl metal precursors are discussed in chapter 6.2. In chapter 6.3, details of the depositions and properties of $LaLuO_3$ films are presented. Finally in chapter 6.4 the results of $Er_xGa_{2-x}O_3$ film depositions are summarized.

6.1 $REScO_3$ thin films

At the time the first $YScO_3$ thin film depositions were carried out, there were practically no other ALD reports published concerning ternary rare earth oxide thin films containing two different rare earth elements. Therefore some of the excellent properties of the $YScO_3$ thin films came as a surprise and encouraged us to continue further investigations of this group of materials. Due to the similarity of the rare earth elements in many aspects and on the other hand the gradual change in their cation size, $REScO_3$ thin films have several similar and gradually evolving properties.

The film thicknesses of all $REScO_3$ films were linearly dependent on the number of the deposition cycles, which is typical for an ALD process. As depicted in Figure 5, the growth rate of the $REScO_3$ films deposited by the thd-process showed linear relationship and an expected trend of increasing growth rate with increasing RE^{3+} cation radius. Similar trend was observed for binary RE_2O_3 thin films deposited by the thd-process.[12] However, the increase in the growth rate can only partly be explained by the increase in the cation radius. For example, the radius of the La^{3+} ion is *ca*. 23 % larger than the radius of the Dy^{3+} cation, but there is *ca*. 44 % increase in growth rate of $LaScO_3$ compared to the growth rate of $DyScO_3$. One possible explanation mentioned earlier by Päiväsaari[74] is based on the fact discussed in chapter 4.2.1, *viz*. the tendency of larger lanthanoids to prefer higher coordination numbers than six and therefore form dimeric thd-complexes. Although gas phase studies of $RE(thd)_3$ show that for many $RE(thd)_3$ the most abundant species in gas phase under high vacuum is $Re(thd)_2^+$,[76] on the surface of the substrate or the growing thin film they may form dimers. This would lead to a denser coverage of the surface and a higher growth rate. The growth rates were linearly dependent on the RE:Sc precursor pulsing ratio, and the measured growth rates followed the theoretical growth rates calculated from the growth rates of binary RE_2O_3

thin films. $DyScO_3$ thin films were deposited also at 350°C, and a growth rate of 0.21 Å/cycle was observed, which is slightly higher than the growth rate at 300°C.

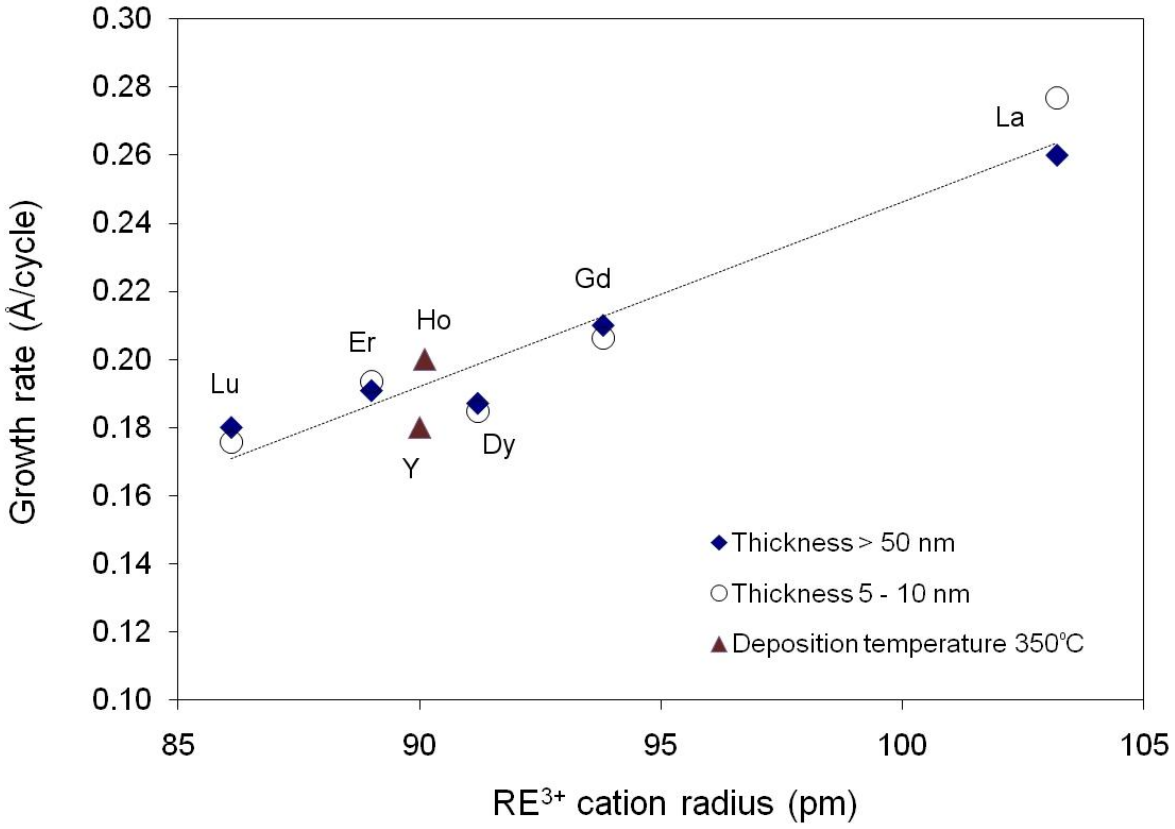

Figure 5. Growth rates of $REScO_3$ thin films as a function of the RE^{3+} cation radius. The deposition temperatures were 300°C except for $YScO_3$ and $HoScO_3$ thin films.

A series of films with different metal precursor pulsing ratios was deposited and after every deposition the actual metal ratio RE:Sc was routinely analyzed by X-ray fluorescence spectroscopy (XRF). Based on these results pulsing ratios for stoichiometric $REScO_3$ thin films were established. According to XRF, small excess of Sc was needed except for $ErScO_3$ and $LuScO_3$. In these cases, it was sufficient that an equal amount of RE and Sc or even a slight excess of RE was pulsed into the reactor. According to RBS, this resulted in slightly Sc rich $YScO_3$, $ErScO_3$ and $LuScO_3$ films, but $RESCO_3$ of larger RE had metal ratio very close to stoichiometric ratio (RE:Sc= 0.97-1.06). Table 7 summarizes the deposition parameters applied for the stoichiometric $RESCO_3$ thin films, observed growth rates and measured metal ratios.

Table 7. Precursor pulsing ratios, growth rates and measured metal ratios of $RE ScO_3$ thin films.

$RE ScO_3$	RE:Sc	growth rate		measured RE:Sc	
	pulsing ratio	< 50 nm (Å/cycle)	> 50 nm (Å/cycle)	XRF	RBS
$LaScO_3$	5:6	0.28	0.26	1 : 0.94	1 : 1.03
$GdScO_3$	5:6	0.21	0.21	1 : 0.96	1 : 0.98
$DyScO_3$	10:11	0.18	0.19	1 : 1.01	1 : 0.94
$HoScO_3$[a]	5:6	-	0.20[a]	1 : 1.01	1 : 1.06[b]
$YScO_3$[a]	10:11	-	0.18[a]	1 : 1.05	1 : 1.22[b]
$ErScO_3$	1:1	0.19	0.19	1 : 0.98	1 : 0.86
$LuScO_3$	6:5	0.18	0.18	1 : 0.99	1 : 0.82

[a] Thin films deposited at 350°C

[b] Metal ratio analyzed by TOF-ERDA

Small amount of carbon was found in all the $RE ScO_3$ films, varying from 2.7 to 0.9 at-% for the larger REs (La-Dy) and ≤ 0.5 at-% for the smaller REs (Ho, Y, Er, Lu,). The type of carbon impurities was studied in more detail by FTIR spectroscopy. As discussed in chapter 4.2.1, the thd-complexes of RE require a strong oxidizer, such as ozone, in order to form oxide thin film, which often results in oxidation of carbon impurities to carbonate. Unidentate carbonate group can easily be identified by its typical doublet band at *ca.* 1500-1400 cm^{-1} and a singlet at *ca.* 850 cm^{-1} in FTIR spectrum.[126] Figure 6 shows how the intensity of the carbonate doublet diminishes as we move from the $LaScO_3$ spectrum to $LuScO_3$ spectrum. This method alone does not give quantitatively the carbonate concentration in the film, but we can, with some certainty, compare the normalized peak areas (*i.e.* peak area divided by the film thickness) of different samples. Figure 6 depicts the normalized peak area as a function of the RE^{3+} cation radius showing a clear trend of increasing concentration of carbonate with increasing cation radius. Other impurities detected by TOF-ERDA were hydrogen and fluorine. The concentration of hydrogen was 0.7-2.3 at-%, and no particular trend was observed related to the cation radius. Similar levels of hydrogen have been observed in binary RE_2O_3 thin films deposited by the thd-process.[12] Fluorine is an element commonly detected in films deposited in this reactor particularly when ozone is used as oxygen source and it is assumed to originate from the vacuum grease or the Teflon gaskets used in the reactor. Metal to oxygen ratios varied from 0.55 to 0.69, indicating nearly ideal stoichiometry or small excess of oxygen. Impurities and metal to oxygen ratios are summarized in Table 8.

Table 8. Summary of impurities and M:O ratios found in $REScO_3$ films determined by TOF-ERDA.

$REScO_3$	**M:O**	**C (at-%)**	**H (at-%)**	**F (at-%)**
$LaScO_3$	0.57	2.7 ± 0.2	1.8 ± 0.1	2.0 ± 0.2
$GdScO_3$	0.65	0.9 ± 0.1	1.9 ± 0.1	2.9 ± 0.2
$DyScO_3$	0.66	1.3 ± 0.3	2.3 ± 0.2	0.7 ± 0.2
$HoScO_3$[a]	0.66	0.2 ± 0.1	0.8 ± 0.1	1.0 ± 0.1
$YScO_3$[a]	0.69	< 0.2	0.7 ± 0.2	0.9 ± 0.1
$ErScO_3$	0.55	0.5 ± 0.1	1.3 ± 0.2	3.8 ± 0.5
$LuScO_3$	0.64	0.4 ± 0.1	1.5 ± 0.1	2.8 ± 0.3

[a] Thin films deposited at 350°C

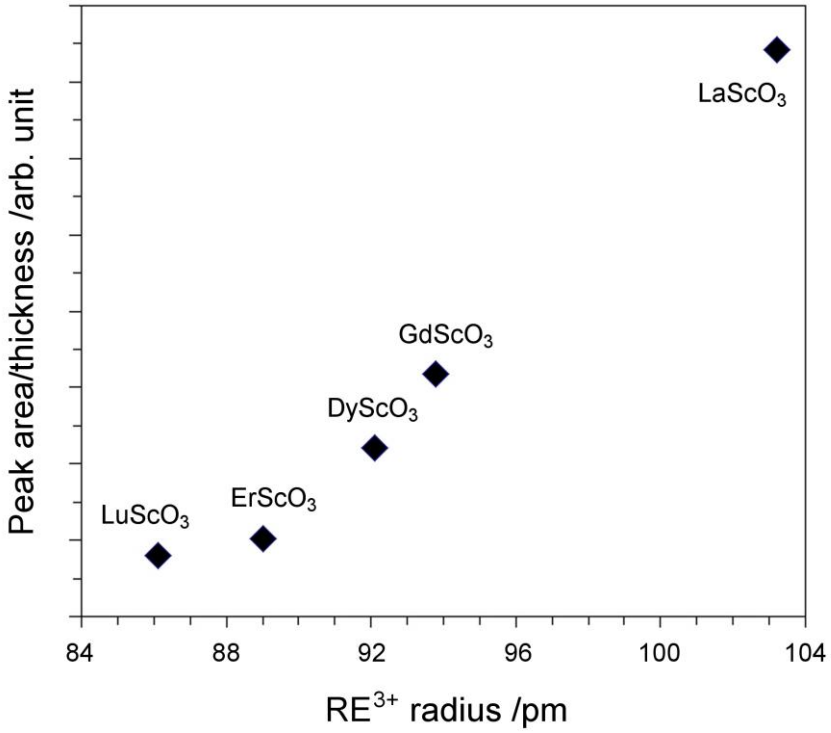

Figure 6. Normalized carbonate doublet peak areas *vs.* RE^{3+} cation radius indicating a clear trend in the amount of carbonate found in $REScO_3$ films.[III]

As discussed in chapter 4.1, $REScO_3$ can crystallize as a solid solution of binary oxides or form a perovskite phase. According to the XRD data, all the $REScO_3$ films with closely stoichiometric composition studied in this thesis were amorphous as-deposited except for $LuScO_3$, which showed weak diffraction peaks of the cubic C-type structure even before thermal annealing. After thermal annealing, all other films also crystallized and formed polycrystalline structures. The radius of the

RE^{3+} cation clearly affected not only the crystallizing phase but also the crystallization temperature. With the larger REs (La and Gd) the films crystallized as perovskite phase at relatively high temperatures (800-900°C), while smaller REs preferred the cubic C-type solid solution. The formation of solid solution was clearly evident in case of $YScO_3$, when several samples with large range of Y:Sc ratio were examined. In Figure 7, a linear relationship can be seen between the d-values of the major diffraction peaks and the relative amount of yttrium in the films indicating a formation of the solid solution.

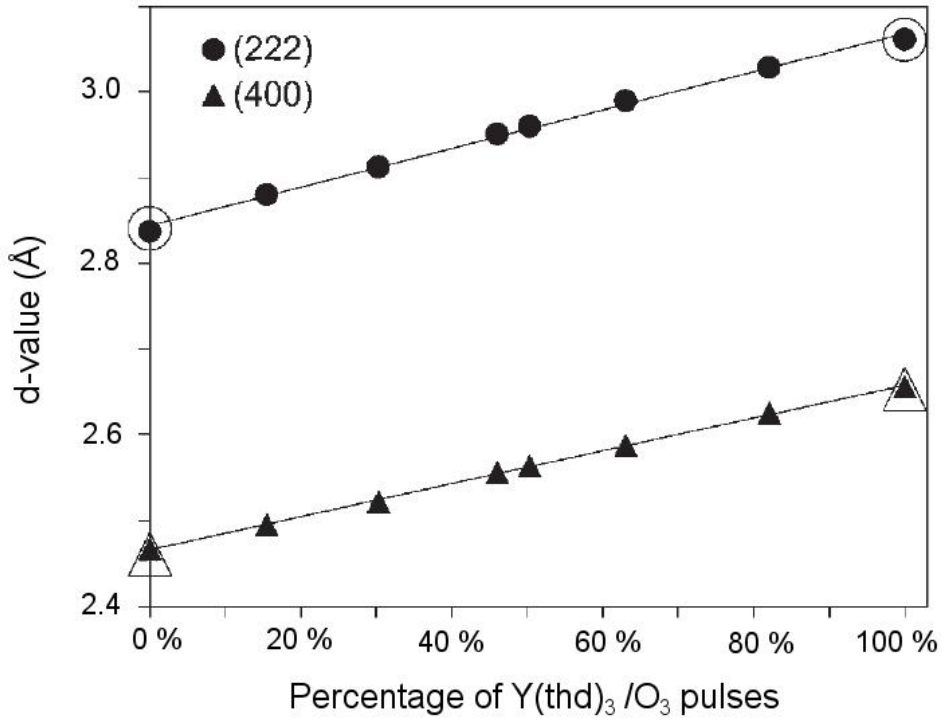

Figure 7. The diffraction peak d-values of $Y_xSc_{2-x}O_3$ thin films as a function of the film composition. Open symbols represent d-values for binary Sc_2O_3 (0 %) and Y_2O_3 (100 %).[I]

The crystallization temperature of the films forming solid solution dropped with decreasing RE^{3+} cation radius from 1000°C for $YScO_3$ to the deposition temperature 300°C for $LuScO_3$. Although $DyScO_3$ first crystallized as solid solution of binary oxides at 900°C, after annealing at 1000°C also peaks of the perovskite phase appeared in the diffraction pattern. Figure 8 shows diffraction patterns of annealed $LaScO_3$, $DyScO_3$ and $LuScO_3$ films. The strongest reflection, *viz.* the (222) reflection of solid solution can easily be identified in the diffraction pattern of $LuScO_3$ at $2\theta = 30.6°$ (d = 2.92 Å) and, due to larger Dy^{3+} cation radius, at $2\theta = 30.4°$ (d = 2.94 Å) for $DyScO_3$. Other strong and easily identified reflections of the C-type structure are (211), (400), (440) and (622), all clearly recognizable in patterns of $LuScO_3$ and $DyScO_3$. For the $LaScO_3$ perovskite phase the strongest reflections seen are (110), (020), (112) and (004). In the region $2\theta = 20\text{-}30°$ of the $DyScO_3$

diffraction pattern there are three peaks, although only one of them belongs to the C-type phase. The other two at 2θ = 22.7° (d = 3.91 Å) and 2θ = 25.5° (d = 3.49 Å), as well as a peak at 2θ = 32.3° (d = 2.77 Å), can be identified as reflections of perovskite $DyScO_3$, indicating that two different crystalline phases are present in $DyScO_3$ film annealed at 1000°C. Similar behaviour was observed for $DyScO_3$ thin films deposited at 350°C. The crystallizing phases and the crystallization temperatures *vs.* the RE^{3+} cation radius are summarized in Figure 9.

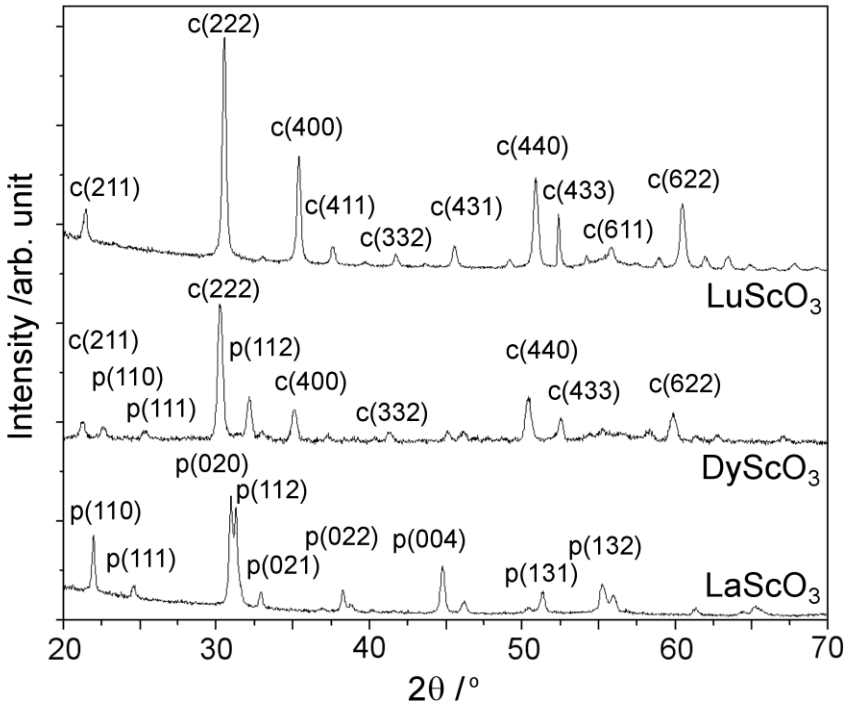

Figure 8. GIXRD patterns of $LaScO_3$ (after annealing at 800°C), $DyScO_3$ (1000°C) and $LuScO_3$ (600°C). $LaScO_3$ crystal structure can be identified as orthorhombic perovskite type and $LuScO_3$ as cubic C-type. Most intense peaks of both phases (labeled "c" for cubic C-type and "p" for perovskite) can be identified in the diffraction patters of $DyScO_3$.[III]

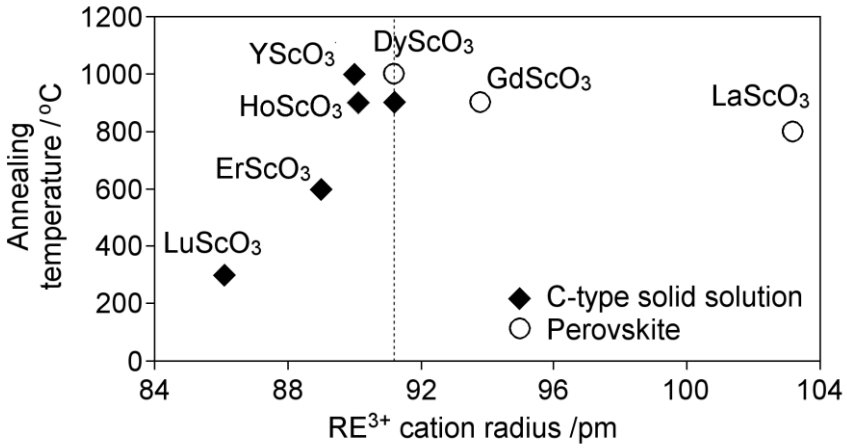

Figure 9. $REScO_3$ crystallization temperatures and phases detected *vs.* the RE^{3+} cation radius.

$YScO_3$ and $GdScO_3$ were analyzed for surface morphology by AFM. Very thin samples (thickness varying from 5 nm to 20 nm) of as-deposited $GdScO_3$ had rms roughnesses of *ca.* 0.3 nm and for thicker (*ca*. 40 nm) samples of $YScO_3$ the rms roughness was below 0.5 nm. Annealing at 800°C had no effect on the surface roughness of the $YScO_3$ thin films. However, annealing at 1000°C produced cracks on the film surface. $GdScO_3$ films were not analyzed for surface morphology after thermal annealing.

For $YScO_3$, Al/$YScO_3$/SiO_2/p-Si(100)/Al capacitor stacks were realized and electrical characterization measurements were carried out both before and after annealing at 800°C. The $YScO_3$ layer thickness was *ca*. 40 nm. Before annealing, a flat band voltage (V_{fb}) shift towards positive direction indicating negative fixed charges was observed, but upon thermal annealing V_{fb} shifted towards negative direction. Hysteresis (ΔV_{fb}) was low before and after annealing. There was a shoulder-like feature in the *C-V* curve of the as deposited film, possibly caused by the interface defects and traps associated with unpassivated silicon dangling bonds.[127] This feature completely disappeared upon annealing. The effective permittivity κ_{eff} calculated from the accumulation capacitance was 14.2 for the as-deposited and 15.0 for the annealed film. These are clearly higher than expected values based on previously published data (9-11) for binary RE_2O_3 films deposited by similar thd-process.[12] The leakage current density was low (~ 10^{-8} A cm^{-2} at 1 V).

For all other $REScO_3$ systems studied except for $HoScO_3$, a series of thin films with thicknesses varying from 5 to 20 nm (and also 55nm for $DyScO_3$) were deposited onto HF-last silicon surface and Pt/$REScO_3$/p-Si(100)/Al capacitor structures were realized. All $REScO_3$ films gave smooth and

featureless *C-V* curves with very low (typically < 35 mV) hysteresis, examples shown in Figure 10. CETs were calculated from the capacitances taken at a gate voltage -2 V and plotted *versus* the physical thicknesses resulting in straight lines, as shown in Figure 11 for $GdScO_3$. The dielectric constants were extracted from the slopes of the CET-figures and are listed in Table 9 along with some other electrical characteristics. The highest dielectric constant was observed for $DyScO_3$ (~24) and the lowest for $LuScO_3$ (~11). The leakage current densities were low, especially for $LuScO_3$ (~10^{-9} A/cm^2). This was somewhat surprising, since thicker $LuScO_3$ films were partly crystalline before any thermal treatment, which usually leads to higher leakage current density. However, the sample analyzed for leakage current was only 5 nm thick, and may have been amorphous, if the crystallization during the deposition only takes place when the film thickness reaches certain critical value. This thickness dependence of crystallization is advantageous for the application as thin gate oxide layers and has also been observed for HfO_2 films grown by ALD; the crystallization temperature of a 5 nm thick film was 600°C, while a 40 nm thick film crystallized already at 430°C.[128]

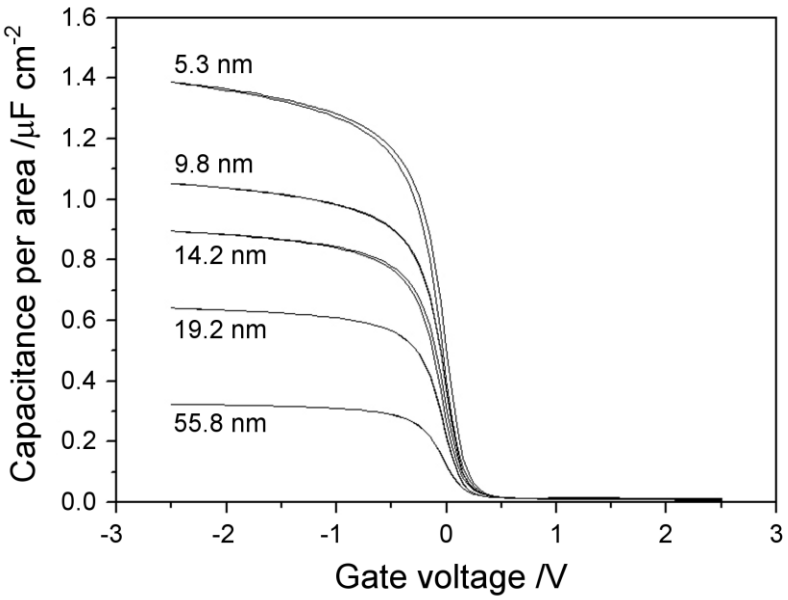

Figure 10. *C–V* curves of $DyScO_3$ films with varying thicknesses.[III]

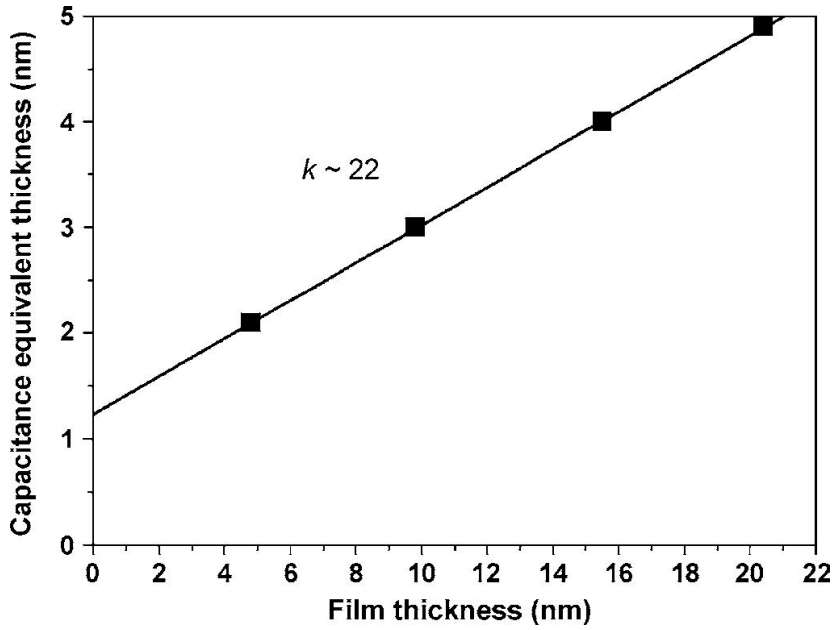

Figure 11. CET vs. physical film thickness for $GdScO_3$ thin films. The dielectric constant κ was extracted from the slope.[II]

Table 9. Electrical properties of $REScO_3$.films. For $YScO_3$ different test structure was employed.

$REScO_3$	**κ**	**Leakage current density (A/cm^2)**	**V_{fb} (V)**	**ΔV_{fb} (mV)**
$LaScO_3$	16	~ 10^{-6}	0.05 – 0.2	10 – 90
$GdScO_3$	22	~ 10^{-6} – 10^{-7}	0.02 – 0.13	≤ 100
$DyScO_3$	24	~ 10^{-7} – 10^{-8}	0.13 – 0.23	10 – 25
$YScO_3$	14[a]	~ 10^{-8}	~0[b]	< 10
$ErScO_3$	18	~ 10^{-4}	-0.03 – 0.4	5 – 30
$LuScO_3$	11	~ 10^{-9}	0.04 – 0.12	5 – 24

[a] κ_{eff}, includes the effect of SiO_2 interfacial layer

[b] Al/insulator/p-Si(100) stack, ideal V_{fb} ~ -1 V

When comparing the dielectric constants of $YScO_3$ and other $REScO_3$ films, it must be noted that slightly different approaches were employed. The effective dielectric constant κ_{eff} of the $YScO_3/SiO_2$ capacitor stack was calculated based on only one capacitance value at accumulation and the effect of the interfacial SiO_2 layer was included while for the other $REScO_3$ a series of films with varying thicknesses were analyzed and the κ was evaluated from a CET plot having 4 of 5

different measurements. Therefore, the κ_{eff} for $YScO_3$ is not fully comparable to the κ values of other $REScO_3$ films. For comparison, similar preliminary characterization of single $GdScO_3$ film having thickness 40.6 nm gave $\kappa \approx 13.6$[28,129] which is a considerably lower value than $\kappa \approx 22$ extracted from the CET plot.

6.2 $YScO_3$ thin films deposited by the Cp-process

Since yttrium is rather small in size, methyl-substituted cyclopentadienyl complex is thermally stable enough to be used as an ALD precursor. Therefore in addition to the thd-process, another precursor system was examined for comparison. The Cp-process yielded a considerably higher growth rate than the thd-process, as expected based on the binary processes. For films with precursor pulsing ratio Y:Sc=1:1, the growth rate was 1.08 Å/cycle for the Cp-processes, while the thd-process gave growth rate of only 0.18 Å/cycle. Figure 12 shows that the observed growth rates for films deposited by the Cp-process are slightly lower than the growth rate directly calculated from the binary oxide growth rates. The growth rates of films deposited by the thd-process are included for comparison. Both processes gave linear relationship between the number of deposition cycles and the film thickness.

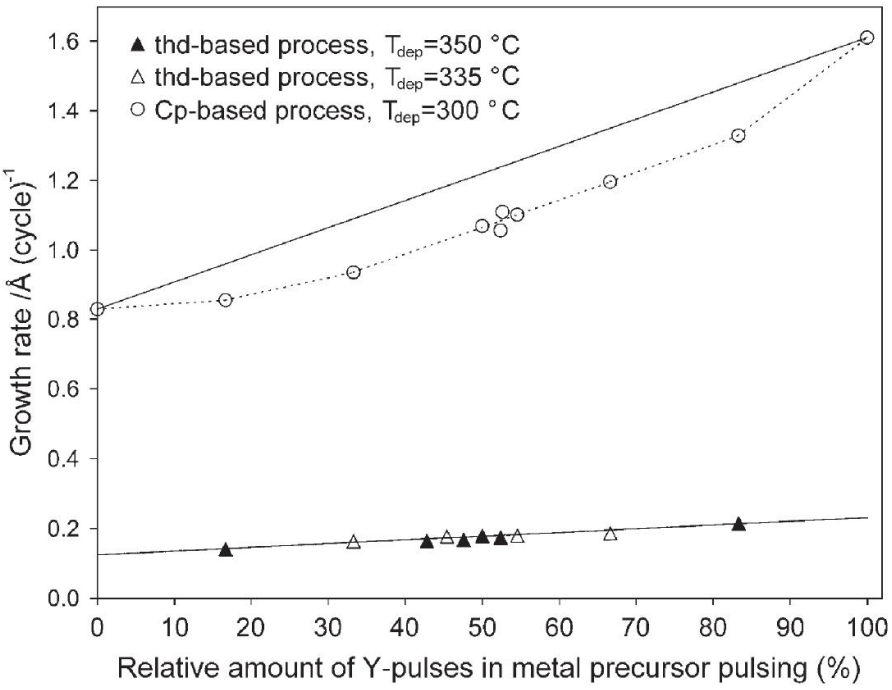

Figure 12. Measured $Y_xSc_{2-x}O_3$ film growth rates and the theoretical growth rates (solid lines) as a function of the Y precursor pulsing.[I]

As in the case of other $REScO_3$ films, controlling the metal ratio Y:Sc was easy and straightforward. With the Cp-precursors an excess of Y was needed in order to deposit stoichiometric $YScO_3$ due to steric hindrance of larger CpMe-ligands giving smaller fraction of a monolayer on each deposition cycle. The Cp-process yielded films with low concentration of impurities, especially carbon levels were low (0.1 at-%). According to TOF-ERDA, the measured metal to oxygen ratio was stoichiometric within the experimental error (M:O = 0.66). The crystallization temperature of $YScO_3$ films deposited by the Cp-process was somewhat lower (800°C) than for films deposited by the thd-process (1000°C), but otherwise very similar crystallization behaviour was observed regardless the precursor system applied.

For the $YScO_3$ films deposited by the Cp-process, similar Al/$YScO_3$/SiO_2/p-Si(100)/Al capacitor stacks were realized for the electrical characterization. Considerably larger hysteresis of *C-V* curve was observed than for the films deposited by the thd-process. Hysteresis in metal-insulator-silicon structures can be caused by several reasons, *e.g.* contamination, structural disorder or other defects in the film or interfaces. However, determining the reason in this case would require more detailed investigation outside the scope of this thesis. The effective permittivity of the as-deposited film was 16, which is considerably higher than what was obtained for binary Y_2O_3 film (κ_{eff} = 10) deposited by the Cp-based ALD process[38] and slightly higher than for the films deposited by the thd-process. However, annealing at 800°C (*i.e.* the crystallization temperature of the films) reduced the κ_{eff} to *ca.* 10. This indicates that the amorphous structure is clearly beneficial when considering $YScO_3$ as a gate oxide for MOSFETs. The leakage current density was slightly higher than what was observed for the film deposited by the thd-process.

6.3 $LaLuO_3$ thin films

In publication IV the properties of $LaLuO_3$ thin films deposited by ALD are presented. In this section the ALD process will be described in more detail. $LaLuO_3$ thin films were deposited at 300°C and 350°C. Otherwise similar deposition conditions as described for $REScO_3$ films were applied, including precursor pulse lengths.

For ternary $LaLuO_3$ thin films the growth rate depended on the deposition temperature. At 300°C a growth rate of 0.26 Å/cycle was observed for stoichiometric $LaLuO_3$ while at 350°C the growth rate was 0.33 Å/cycle. It appears that the increase is mainly due to the temperature dependence of the

lanthanum oxide growth rate by the thd-process. According to an earlier study,[68] the growth rate of binary La_2O_3 thin films grown by the thd-process remains constant at 0.36 Å/cycle at the deposition temperatures 250-275°C, but increases at higher deposition temperatures. However, increasing the precursor pulse length did not affect the growth rate and a linear relationship between the number of deposition cycles and the film thickness was observed even at 375°C, indicating surface controlled growth. In this study, for binary Lu_2O_3 a constant growth rate of 0.19 Å/cycle was observed at temperatures 300-350°C. There was also a relationship between the growth rate and the metal precursor pulsing ratio; higher proportion of lanthanum yielded higher growth rate.

The temperature dependence of the lanthanum deposition rate had only a slight effect on the metal ratio of the films deposited at different temperatures, as shown in Figure 13. According to XRF, at 300°C the stoichiometric metal ratio La:Lu ≈ 1 was achieved with metal pulsing ratio La:Lu = 7:8. At 350°C slightly higher proportion of lutetium was needed and metal precursor pulsing ratio La:Lu = 3:4 resulted in stoichiometric metal ratio. Only films deposited at 300°C were analyzed by RBS and La:Lu ratios varying from 1:0.99 to 1:1.03 were found. However, the films contained considerable amount of excess oxygen corresponding formula $LaLuO_{5.2}$. Annealing at 800°C reduced some but not all of the excess oxygen resulting in formula $LaLuO_{3.6}$.

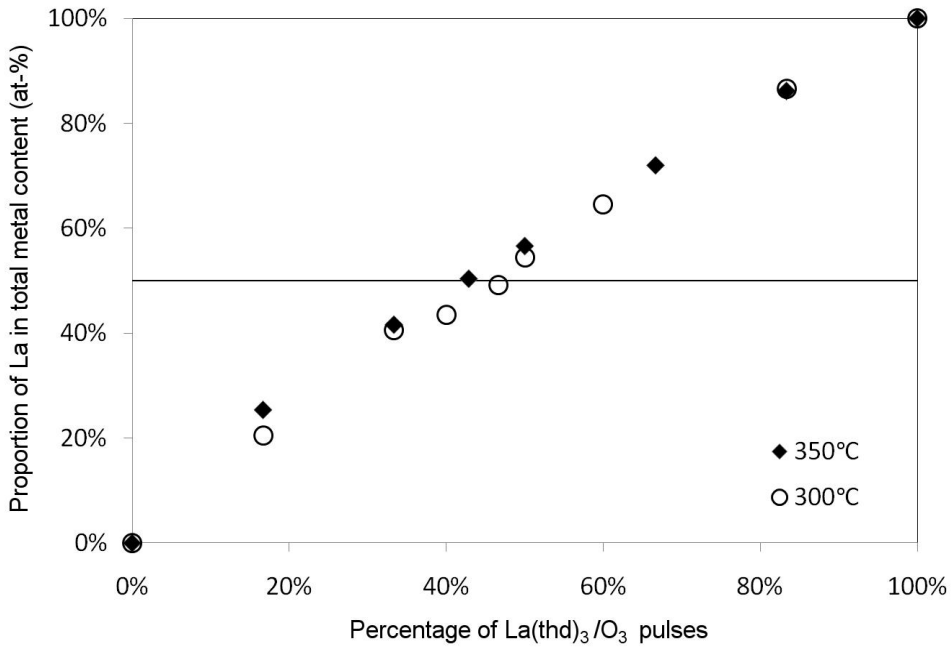

Figure 13. Metal composition of $La_xLu_{2-x}O_3$ thin films as a function of the metal precursor pulse ratio (0 % indicating binary Lu_2O_3 deposition and 100 % binary La_2O_3 deposition) at two different deposition temperatures. Solid line represents the stoichiometric composition $LaLuO_3$. The metal ratios were determined by XRF.

Previous studies of La_2O_3[68] and $LaScO_3$[III] had shown that the lanthanum containing thin films deposited by the thd-process often contain carbonate. Therefore the $LaLuO_3$ films were examined by FTIR. Also the effect of higher deposition temperature 350°C was examined. The $LaLuO_3$ films deposited at 300°C and 350°C were analyzed before and after thermal annealing and the intensities of the carbonate doublet band (at *ca.* 1500-1400 cm^{-1}) were compared. The preliminary results indicate that films deposited at 350°C indeed have lower carbonate concentration, and the annealing reduced the carbonate concentration regardless the deposition temperature. However, more detailed analysis is needed by truly quantitative methods such as TOF-ERDA. Also the possible relationship between the carbonate and excess oxygen in $LaLuO_3$ films needs more detailed investigation.

The deposition temperature did not affect the crystallization behaviour of the $LaLuO_3$ thin films and the as-deposited $LaLuO_3$ thin films were amorphous regardless the deposition temperature. The crystallization occurred during 10 minutes annealing at 900°C under flowing nitrogen and an orthorhombic $LaLuO_3$ phase was found (Figure 14.) Oxygen annealing resulted in crystallization at lower temperature, *viz.* 800°C. However, when a very short (10 s) oxygen annealing was applied, the onset of crystallization was at 1100°C. This meets the requirements for future high-κ dielectric materials listed in Table 1. The same crystallization onset temperature was observed for thin (11 nm) $LaLuO_3$ film deposited by PLD.[118]

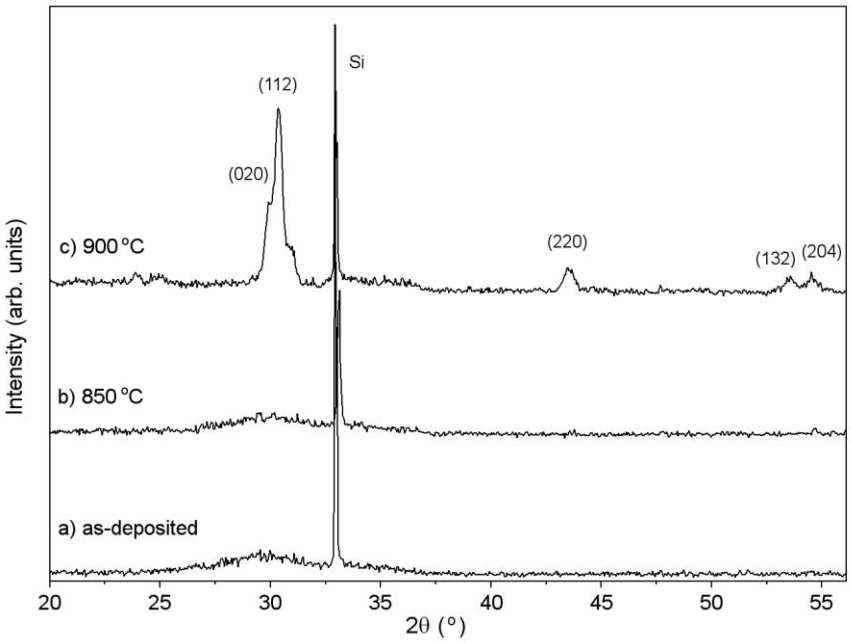

Figure 14. X-ray diffraction patterns of $LaLuO_3$ film with stoichiometric metal ratio a) as-deposited and annealed at b) 850°C and c) 900°C for 10 minutes under flowing nitrogen. The film thickness is *ca.*100 nm.

A series of thin $LaLuO_3$ samples deposited at 300°C with thicknesses varying from 6 nm to 72 nm were analyzed for electrical characterization. The C-V curves measured after 10 min annealing at 600°C under oxygen were smooth and free of hysteresis. However, the dielectric constant extracted from the CET-plot was lower than expected, *viz.* only 17 for the as-deposited samples and 20 after oxygen annealing at 600°C. Oxygen annealing at 700°C did not give any significant change in κ, but annealing at 800°C resulted in further improvement. Thinner (6-17 nm) samples gave $\kappa \approx 25$, but for the thickest sample (*ca.* 60 nm) a desired value $\kappa \approx 30$ was observed. However, as already mentioned the annealing at 800°C also caused phase transformation from amorphous to crystalline orthorhombic $LaLuO_3$, which may lead to leakage current problems. For the thinnest sample (6 nm) a leakage current density below 10^{-6} A/cm^2 was measured.

6.4 $Er_xGa_{2-x}O_3$ thin films

As discussed in chapter 2.5, Gd was found to have beneficial effect on Ga_2O_3 as possible gate oxide in GaAs MOSFETs. The reason for this was thought to be the electropositive nature of Gd, and it was suggested that other RE elements could have similar effect. In this thesis deposition of $Er_xGa_{2-x}O_3$ with two different precursor systems was studied. However, only silicon was used as a substrate due to complexity of the electrical characterization of Ga-based structures.

Analogous to the $YScO_3$ films, considerably higher growth rate was achieved by using amidinate and cyclopentadienyl metal precursor compared to the thd-process. For the films deposited by the thd-process, the growth rate varied only slightly (0.24-0.28 Å/cycle) depending on the film composition and the values were in good accordance with the theoretical growth rates calculated from the parent binary processes. For films deposited by the amidinate and Cp-precursors, a constant growth rate (0.95-1.00 Å/cycle) was observed for Er pulse percentages of up to about 70 %. With higher Er pulse percentages the growth rate increased from *ca.* 1 to *ca.* 1.5 Å/ cycle, which equals to the growth rate of the binary Er_2O_3 process. With both processes the measured percentages of erbium were slightly lower than the percentage of Er pulses and pulsing ratio Er:Ga=1:1 resulted in $Er_xGa_{2-x}O_3$ with x=0.71 and x=0.76 for the thd- and the Cp/amidinate-processes, respectively. For the thd-process, this can be explained by the smaller ligand size of the Ga-precursor, resulting in larger fraction of monolayer per cycle. For the Cp/amidinate-process, the dimeric structure of $Ga_2(NMe_2)_6$ may lead to higher surface density, although it is not clear whether $Ga_2(NMe_2)_6$

sublimes as monomeric or dimeric species.[130] The films contained stoichiometric or nearly stoichiometric amount of oxygen. Only very small amount of impurities were found in films deposited by the thd-process, but 2.0-6.1 at-% of carbon and 5.0-10.3 at-% of hydrogen was found in films deposited by the Cp/amidinate-process, both concentrations decreasing with an increase in the erbium content. Especially the carbon content is higher than expected, since the binary Ga_2O_3 thin film deposited by the amidinate-process at 250°C contained only 1.0 at-% of carbon[130] and Er_2O_3 film deposited by the Cp-process less than 0.3 at-% of carbon.[81] Hydrogen concentrations found in binary films were 4.8 at-% and 2.9 at-% for the Ga_2O_3 and the Er_2O_3 films, respectively.

The crystal structure of the films was examined before and after thermal annealing. The $Er_xGa_{2-x}O_3$ films can adopt different structures; therefore samples with varying x were analyzed. Regardless the x and the precursor system used, all as-deposited samples were amorphous. For films deposited by the thd-process, crystallization occurred upon annealing at 900-1000°C under flowing nitrogen, either as $Er_3Ga_5O_{12}$ or as a mixture of β-Ga_2O_3 and $Er_3Ga_5O_{12}$. An $Er_xGa_{2-x}O_3$ film with x = 1.12 (pulsing ratio Er:Ga 11:5) remained amorphous at 900C but crystallized as $Er_3Ga_5O_{12}$ upon annealing at 1000°C. Slightly more gallium rich film having x = 0.71 (corresponding formula $Er_{2.84}Ga_{5.16}O_{12}$), crystallized as $Er_3Ga_5O_{12}$ at 900°C. Small shift of the d-values towards lower values was detected which could be explained by a part of smaller Ga^{3+} cations replacing the larger Er^{3+} cations in the lattice. Film having even higher portion of Ga deposited with pulsing ratio Er:Ga = 3:10 crystallized as a mixture of β-Ga_2O_3 and $Er_3Ga_5O_{12}$ at 900°C, but the diffraction peaks were broad and low in intensity, indicating poor crystallinity.

Crystallization behaviour of the $Er_xGa_{2-x}O_3$ films deposited with Cp- and amidinate-precursors was not as straightforward as for films deposited with the thd-precursors. Film having x = 0.76 (corresponding formula $Er_{3.04}Ga_{4.96}O_{12}$) crystallized as $Er_3Ga_5O_{12}$ at 900°C, as expected. Film having higher portion of Ga (x = 0.35, formula $Er_{1.4}Ga_{6.6}O_{12}$), on the other hand, did not show any signs of crystallization even after annealing at 1000°C even though film deposited with the thd-process having very similar composition had crystallized as a mixture of β-Ga_2O_3 and $Er_3Ga_5O_{12}$ at 900°C. Higher concentration of impurities may have prevented this sample from crystallizing. An $Er_xGa_{2-x}O_3$ film that was grown with 3:1 Er:Ga pulsing ratio and annealed at 1000°C afforded a diffraction pattern containing reflections consistent with both β-Ga_2O_3 and $Er_3Ga_5O_{12}$ and also some reflections too broad and of too low intensity to be identified. The presence of β-Ga_2O_3 was somewhat surprising since the film (x = 1.21 corresponding with the formula $Er_{4.84}Ga_{3.16}O_{12}$)

contained less gallium than films described above. Diffraction peaks were also quite broad indicating poorly crystalline structure. An overview of the crystallization behaviour of the $Er_xGa_{2-x}O_3$ thin films is presented in Table 10.

Table 10. Summary of the crystallization behaviour of $Er_xGa_{2-x}O_3$ thin films. Unless otherwise noted, the film composition (x) was determined by RBS.

	Er:Ga	**x**	**Formula**	**T_{cryst} (°C)**	**Phase**
$Er(thd)_3$,	11:5	1.12	$Er_{4.48}Ga_{3.52}O_{12}$	1000	$Er_3Ga_5O_{12}$
$Ga(acac)_3$, O_3	1:1	0.71	$Er_{2.84}Ga_{5.16}O_{12}$	900	$Er_3Ga_5O_{12}$, shifted d-values
	3:10	0.27[a]	$Er_{1.08}Ga_{6.92}O_{12}$	900	$Er_3Ga_5O_{12}$ + β-Ga_2O_3
$Er(C_5H_4Me)_3$,	3:1	1.21	$Er_{4.84}Ga_{3.16}O_{12}$	1000	$Er_3Ga_5O_{12}$ +
$Ga_2(NMe_2)_6$,					β-Ga_2O_3
H_2O	1:1	0.76	$Er_{3.04}Ga_{4.96}O_{12}$	900	$Er_3Ga_5O_{12}$
	1:3	0.35	$Er_{1.40}Ga_{6.60}O_{12}$	-	-

[a]Determined by XRF

According to AFM, the as-deposited films had smooth and featureless surface regardless of the precursor system used. Typical root mean square (rms) surface roughnesses were all below 1.0 nm. Films were not analyzed after thermal annealing.

$Er_xGa_{2-x}O_3$ is a potential dielectric material for Ga-based microelectronic devices. However, electrical characterization of a *e.g.* GaAs-based MOS-capacitor is much more complicated than that of a silicon-based capacitor. Therefore, Al/$Er_xGa_{2-x}O_3$/SiO_2/p-Si(100)/Al test structure was constructed to analyze some electrical properties of these films. Two samples deposited by each process were chosen and details of the results are presented in Table 11.

Table 11. Summary of the electrical properties of the $Er_xGa_{2-x}O_3$ films

Precursor System	**x**	**thickness (nm)**	**V_{fb} (V)**	**ΔV_{fb} (mv)**	**κ**	**Leakage current density (nA/cm^2)**
$Er(thd)_3$,	0.36	48.6	-0.3	~15	10.8	16
$Ga(acac)_3$, O_3	1.12	45.6	-1.3	~15	11.3	16
$Er(C_5H_4Me)_3$,	0.35	41.4	-0.2	680	9.2	26
$Ga_2(NMe_2)_6$, H_2O	0.76	42.6	-1.2	250	10.4	17

As can be seen in Table 11, with both precursor systems the films which have higher concentration of Er (x = 1.12 and x = 0.76 for the films deposited by the thd- and the Cp/amidinate-process, respectively) have flat band voltage close to -1 V, which is characteristic of ideal Al/insulator/p-Si(100) structures.[131] However, films with lower concentration of Er show flat band voltage shift towards positive direction, which may be an indication of negative fixed charges in the films.

7. Conclusions

Ternary rare earth oxide thin films $REScO_3$ (RE = La, Gd, Dy, Ho, Y, Er and Lu) and $LaLuO_3$ were successfully deposited by ALD utilizing β-diketonate metal precursors and ozone. $YScO_3$ thin films were also deposited by using novel cyclopentadienyl metal precursors and water. The as-deposited, stoichiometric films were amorphous except for $LuScO_3$ and had low level of impurities. Due to the similarity of REs in many aspects and on the other hand the gradual diminishing of RE^{+3} cation radius with increasing atomic number, several gradually evolving deposition characteristics (*e.g.* growth rate) and $REScO_3$ film properties (*e.g.* crystallization temperature) were found. The films crystallized upon annealing as a solid solution of C-type RE_2O_3 oxides or as a perovskite type structure. The crystallization temperatures varied from 300°C ($LuScO_3$) to 900-1000°C (mid-range $REScO_3$, *e.g.* $YScO_3$ and $DyScO_3$). The as-deposited amorphous films had promising electrical properties including high dielectric constant, small hysteresis and low leakage current density. For $LaLuO_3$ thin films the dielectric constant was further increased by thermal annealing and a high dielectric constant of $\kappa \approx 30$ was achieved. However, several aspects of the $LaLuO_3$ thin film depositions such as the unexpectedly high concentration of excess oxygen as detected by RBS and XPS require a more detailed examination. Quantitative analysis of impurities *e.g.* carbon is needed as only preliminary determination of carbonate in the $LaLuO_3$ films was presented in this thesis.

The relationship between the dielectric constant and the crystal structure of the thin film was examined more closely and a pattern was found. In general, thermal annealing increases the dielectric constant of $REScO_3$ and $LaLuO_3$ thin films, but upon crystallization different behaviour is observed depending on the phase formed. For those $REScO_3$ films that crystallized as a solid solution of binary oxides the dielectric constant decreased upon crystallization and equaled that of the binary RE_2O_3 oxides ($\kappa \approx 10$).[12] $YScO_3^{I}$ and $LuScO_3^{III}$ were examples of this behaviour. However, if the film adopted the perovskite type structure, the dielectric constant increased upon

crystallization. This was particularly evident for the $LaLuO_3$ films.[IV]

$Er_xGa_{2-x}O_3$ is a potential gate oxide material for Ga-based compound semiconductor MOSFETs. $Er_xGa_{2-x}O_3$ thin films with varying composition were deposited by ALD for the first time and two different precursor systems were exploited. In addition to β-diketonate metal precursors and ozone, novel cyclopentadienyl and amidinate compounds were used together with water as precursors. For $Er_xGa_{2-x}O_3$ and also for $YScO_3$ the choice of precursors obviously has an influence on the deposition parameters and process characteristics (*e.g.* growth rate) but also on several properties of the thin films including crystallization behaviour and electrical properties. The as-deposited films were amorphous and had dielectric constant $\kappa \approx 9\text{-}11$. Higher concentration of erbium resulted in lower flat band voltage shift (towards positive bias) indicating lower concentration of negative fixed charges. This behaviour is consistent with the assertion that the rare earth metal prevents the formation of gallium suboxides, which would provide a source of negative fixed charge.

References

1. K. Mistry, C. Allen, C. Auth, B. Beattie, D. Bergstrom, M. Bost, M. Brazier, M. Buehler, A. Cappellani, R. Chau, C.-H. Choi, G. Ding, K. Fischer, T. Ghani, R. Grover, W. Han, D. Hanken, M. Hattendorf, J. He, J. Hicks, R. Huessner, D. Ingerly, P. Jain, R. James, L. Jong, S. Joshi, C. Kenyon, K. Kuhn, K. Lee, H. Liu, J. Maiz, B. McIntyre, P. Moon, J. Neirynck, S. Pae, C. Parker, D. Parsons, C. Prasad, L. Pipes, M. Prince, P. Ranade, T. Reynolds, J. Sandford, L. Shifren, J. Sebastian, J. Seiple, D. Simon, S. Sivakumar, P. Smith, C. Thomas, T. Troeger, P. Vandervoorn, S. Williams, K. Zawadzki, *Proc. International Electron Devices Meeting 2007, IEDM Tech. Dig.* (2007) 247.

2. C. Zhao, T. Witters, B. Brijs, H. Bender, O. Richard, M. Caymax, T. Heeg, J. Schubert, V.V. Afanas'ev, A. Stesmans, D.G. Schlom, *Appl. Phys. Lett.* **86** (2005) 132903.

3. M. Wagner, T. Heeg, J. Schubert, C. Zhao, O. Richard, M. Caymax, V.V. Afanas'ev, S. Mantl, *Solid-State Electron.* **50 (**2006) 58.

4. M. Wagner, T. Heeg, J. Schubert, St. Lenk, S. Mantl, C. Zhao, M. Caymax, S. De Gendt, *Appl. Phys. Lett.* **88** (2006) 172901.

5. S. Van Elshocht, P. Lehnen, B, Seitzinger, A. Abrutis, C. Adelmann, B. Brijs, M. Caymax, T. Conard, S. De Gendt, A. Franquet, C. Lohe, M. Lukosius, A. Moussa, O. Richard, P. Williams, T. Witters, P. Zimmerman, M. Heyns, *J. Electrochem.Soc*. **153** (2006) F219.

6. R. Thomas, P. Ehrhart, M. Luysberg, M. Boese, R. Waser, M. Roeckerath, E. Rije, J. Schubert, S. Van Elshocht, M. Caymax, *Appl. Phys. Lett*. **89** (2006) 232902.

7. R. Thomas, J.J. Saavedra-Arias, N.K. Karan, N.M. Murari, R.S. Katiyar, P. Ehrhart, R. Waser, *Solid State Commun* **147 (**2008) 332.

8. M. Roeckerath, J.M.J. Lopes, T. Heeg, J.Schubert, St. Lenk, S.Mantl, *Proc. 9th International Conference on Ultimate Integration of Silicon*, Udine, Italy, 2008, p. 115.

9. M. Leskelä, M. Ritala, *Thin Solid Films* **409** (2002) 138.

10. S.M. George, *Chem. Rev.* **110** (2010) 111.

11. M. Knez, K. Nielsch, L. Niinistö, *Adv. Mater.* **19** (2007) 3425.

12. J. Päiväsaari, M. Putkonen, L. Niinistö, *Thin Solid Films* **472** (2005) 275.

13. F.T. Edelmann, *Chem. Soc. Rev.* **38** (2009) 2253.

14. A.P. Milanov, R.A. Fischer, A. Devi, *Inorg. Chem.* **47** (2008) 11405.

15. J.E. Lilienfeld, *US Patent No. 1,900,018* (1928)

16. D. Kahng, *US Patent 3,102,230* (1960)

17. G. E. Moore, *Electronics* **38** (1965) 114.

18. G. Moore, *Proc. International Electron Devices Meeting 1975, IEDM Tech. Dig.* (1975) 11.

19. S. Thompson, N. Anand, M. Armstrong, C. Auth, B. Arcot, M. Alavi, P. Bai, J. Bielefeld, B.

Bigwood, J. Brandenburg, M. Buehler, S. Cea, V. Chikarmane, C. Choi, R. Frankovic, T. Ghani, G. Glass, W. Han, T. Hoffmann, M. Hussein, P. Jacob, A. Jain, C. Jan, S. Joshi, C. Kenyon, J. Klaus, S. Klopcic, J. Luce, Z. Ma, B. Mcintyre, K. Mistry, A. Murthy, P. Nguyen, H. Pearson, T. Sandford, R. Schweinfurth, R. Shaheed, S. Sivakumar, M. Taylor, B. Tufts, C. Wallace, P. Wang, C. Weber, M. Bohr, *Proc. International Electron Devices Meeting 2002, IEDM Tech. Dig.* (2002) 61.

20. H. S. Momose, M. Ono, T. Yoshitomi, T. Ohgum, S. Nakamura, M. Saito, H. Iwai, *Proc. International Electron Devices Meeting 1994, IEDM Tech. Dig.* (1994) 593.

21. M. Houssa, L. Pantisano, L.-Å. Ragnarssona, R. Degraeve, T. Schram, G. Pourtois, S. De Gendt, G. Groeseneken, M.M. Heyns, *Mater. Sci. Eng. R* **51** (2006) 37.

22. G.D. Wilk, R.M. Wallace, J.M. Anthony, *J. Appl. Phys.* **89** (2001) 5243.

23. J. Robertson, *Rep. Prog. Phys.* **69** (2006) 327.

24. J. Robertson, P.W. Peacock, in: M. Houssa (Ed.), *High-k Gate Dielectrics*, IOP Publishing, London, 2004, p. 372-395.

25. J. Robertson, *J. Vac. Sci. Technol. B* **18** (2000) 1785.

26. R. Chau, S. Datta, M. Doczy, B. Doyle, J. Kavalieros, M. Metz, *IEEE Electron Device Lett.* **25** (2004) 408.

27. E. P. Gusev, C. Cabral Jr., M. Copel, C. D'Emic, M. Gribelyuk, *Microelectron. Eng.* **69** (2003) 145.

28. J. Niinistö, *Atomic Layer Deposition of of High-κ Dielectrics from Novel Cyclopentadienyl-type Precursors*, Doctoral dissertation, Helsinki University of Technology, Espoo 2006, 72 p.

29. P. Lysaght, B. Foran, S. Stemmer, G. Bersuker, J. Bennett, R. Tichy, L. Larson, H.R. Huff, *Microelectron. Eng.* **69** (2003) 182.

30. K.-J. Choi, J.-H. Kim, S.-G. Yoon, W.-C Shin, *J. Vac. Sci. Technol. B* **22** (2004) 1755.

31. M. R. Visokay, J. J. Chambers, A. L. P. Rotondaro, A. Shanware, L. Colombo, *Appl. Phys. Lett.* **80** (2002) 3183.

32. M.S. Akbar, S. Gopalan, H.J. Cho, K. Onishi, R. Choi, R. Nieh, C.S. Kang, Y.H. Kim, J. Han, S. Krishnan, J.C. Lee, *Appl. Phys. Lett.* **82** (2003) 1757.

33. J. Niinistö, M. Putkonen, L. Niinistö, S.L. Stoll, K. Kukli, T. Sajavaara, M. Ritala, M. Leskelä, *J. Mater. Chem.* **15** (2005) 2271.

34. T. Wang, J.G. Ekerdt, *Chem. Mater.* **21** (2009) 3096.

35. Intel press release http://www.intel.com/pressroom/archive/releases/2007/20071025corp.htm (15.6.2010)

36. M. Gurvitch, L. Manchanda, J.M. Gibson, *Appl. Phys. Lett.* **51** (1987) 919.

37. J. Kwo, M. Hong, A.R. Kortan, K.T. Queeney, Y.J. Chabal, J.P. Mannaerts, T. Boone, J.J. Krajewski, A.M. Sergent, J.M. Rosamilia, *Appl. Phys. Lett.* **77** (2000) 130.

38. J. Niinistö, M. Putkonen, L. Niinistö, *Chem. Mater.* **16** (2004) 2953.

39. T. Hattori, T. Yoshida, T. Shiraishi, K. Takahashi, H. Nohira, S. Joumori, K. Nakajima, M. Suzuki, K. Kimura, I. Kashiwagi, C. Ohshima, S. Ohmi, H. Iwai, *Microelectron. Eng.* 72 (2004) 283.

40. V.V. Afanas'ev, A. Stesmans, C. Zhao, M. Caymax, T. Heeg, J. Schubert, Y. Jia, G.D. Schlom, G. Lucovsky, *Appl. Phys. Lett.* **85** (2004) 5917.

41. N. Basu, K.N. Bhat, *J. Appl. Phys.* **63** (1988) 5500.

42. H.-H. Wang, D.-W. Chou, Y.-H. Wang, M.-P. Houng, *Phys. Scr.* **T79** (1999) 239.

43. M. Passlac, E.F. Schubert, W.S. Hobson, M. Hong, N. Moriya, S.N.G. Chu, K. Konstadinidis, J.P. Mannaerts, M.L. Schnoes, G.J. Zydzik, G. J. *J. Appl. Phys.* **77** (1995) 686.

44. J. Kwo, D.W. Murphy, M. Hong, R.L. Opila, J.P. Mannaerts, A.M. Sergent, *Appl. Phys. Lett.* **75** (1999) 1116.

45. M. Hong, J. Kwo, A. R. Kortan, J. P. Mannaerts, A. M. Sergent, *Science* **283** (1999) 1897.

46. K.-H. Kwon, J.-K. Yang H.-H. Park, J. Kim, T.M. Roh, *Appl. Surf. Sci.* **252** (2006) 7624.

47. P.D. Ye, G.D. Wilk, J. Kwo, B. Yang, H.-J.L. Gossmann, M. Frei, S.N.G. Chu, J P. Mannaerts, M. Sergent, M. Hong, K.K. Ng, J. Bude, *IEEE Electron Device Lett.* **24** (2003) 209.

48. T. Suntola, J. Antson, *US Patent No. 4,058,430* (1977).

49. J. Päiväsaari, J. Niinistö, P. Myllymäki, C. Dezelah, C.H. Winter, M. Putkonen, M. Nieminen, L. Niinistö, *Top. Appl. Phys.* **106** (2007) 15.

50. N.N. Greenwood and A. Earnshaw, *Chemistry of the Elements*, 2nd Ed., Butterworth-Heinemann, Oxford 1997, pp.1227-1249.

51. R.G. Haire and L. Eyring, in: *Handbook on the Physics and Chemistry of Rare Earths*, vol. 18 (Eds. K.A. Gschneider Jr., L. Eyring, G.R. Choppin, G.H. Lander), Elsevier, Amsterdam 1994, p. 413-505.

52. R.P. Liferovich, R.H. Mitchell, *J. Solid State Chem.* **177** (2004) 2188.

53. J.B. Clark, P.W. Richter, L. du Toit, *J. Solid State Chem.* **23** (1978) 129.

54. T. Heeg, M. Roeckerath. J. Schubert, W. Zander, Ch. Buchal, H.Y. Chen, C.L. Jia, Y. Jia, C. Adamo, D.G. Schlom, *Appl. Phys. Lett.* **90** (2007) 192901.

55. H.M. Cristen, G.E. Jellison Jr., I. Ohkubo, S. Huang, M.E. Reeves, E. Cicerrella, J.L. Freeouf, Y. Jia, D.G. Schlom, *Appl. Phys. Lett.* **88** (2006) 262906.

56. M. Putkonen and L. Niinistö, *Top. Organomet. Chem.* **9** (2005) 125.

57. K. Kukli, M. Ritala, J. Aarik, T. Uustare and M. Leskelä, *J. Appl. Phys.* **92** (2002) 1833.

58. J. Aarik, A. Aidla, T. Uustare and V. Sammelselg, *J. Cryst. Growth* **148** (1995) 268.

59. K. Binnemans in: *Handbook on the Physics and Chemistry of Rare Earths*, vol. 35 (Eds. K.A. Gschneider Jr., J.-C.G. Bünzli, V.K. Pecharsky), Elsevier, Amsterdam 2005, pp. 107-272.

60. G. Urbain, *Comp. Rend.* **124** (1897) 618.

61. M. Leskelä, L. Niinistö, E. Nykänen, P. Soininen, M. Tiitta, *J. Less-Common Met.* **153** (1989) 219.

62. H. Mölsä, L. Niinistö, M. Utriainen, *Adv. Mater. Opt. Electron.* **4** (1994) 389.

63. H. Mölsä, L. Niinistö, *Mater. Res. Soc. Symp. Proc.* **335** (1994) 341.

64. H. Seim, M. Nieminen, L. Niinistö, H. Fjellvåg, L.-S. Johansson, *Appl. Surf. Sci.* **112** (1997) 243.

65. M. Putkonen, M. Nieminen, J. Niinistö, T. Sajavaara, L. Niinistö, *Chem. Mater.* **13** (2001) 4701-4707.

66. M. Putkonen, T. Sajavaara, L.-S. Johansson, L. Niinistö, *Chem. Vap. Dep.* **7** (2001) 44-50.

67. E.P. Gusev, E. Cartier, D.A. Buchanan, M. Gribelyuk, M. Copel, H. Okorn-Schmidt, C. D'Emic, *Microelectron. Eng.* **59** (2001) 341.

68. M. Nieminen, M. Putkonen, L. Niinistö, *Appl. Surf. Sci.* **174** (2001) 155.

69. T.T. Van, J.P. Chang, *Appl. Surf. Sci.* **246** (2005) 250.

70. T.T. Van, J.P. Chang, *Appl. Phys. Lett.* **87** (2005) 011907.

71. T.T. Van, J.P. Chang, *Surf. Sci.* **596** (2005) 1.

72. A. Kosola, J. Päiväsaari, M. Putkonen, L. Niinistö, *Thin Solid Films* **479** (2005) 152.

73. J. Niinistö, N. Petrova, M. Putkonen, L. Niinistö, K. Arstila, T. Sajavaara, *J. Cryst. Growth* **285** (2005) 191.

74. J. Päiväsaari, *Atomic Layer Deposition of Lanthanide Oxide Thin Films*, Doctoral dissertation, Helsinki University of Technology, Espoo 2006, 69 p.

75. L.I. Martynenko, N.P. Kuz'mina, A.N. Grigor'ev, *Russian J. Inorg. Chem.* **43** (1998) 1038.

76. M. Leskelä, L. Niinistö, E. Nykänen, P. Soininen, M. Tiitta, *Thermochim. Acta* **175** (1991) 91.

77. T. Leskelä, K. Vasama, G. Härkönen, P. Sarkio, M. Lounasmaa, *Adv. Mater. Opt.Electron.* **6** (1996) 169.

78. J. Wilkinson, J.m. Birmingham, *J. Am. Chem. Soc.* **76** (1954) 6210.

79. G. Scarel, A. Debenarbi, D. Tsoutsou, S. Spiga, S. C. Capelli, L. Lamagna, S. N. Volkos, M. Alia, M. Fanciulli, *Appl. Phys. Lett.* **91** (2007) 102901.

80. D. Tsoutsou, G. Scarel, A. Debenarbi, S. C. Capelli, S. N. Volkos, L. Lamagna, S. Schamm, P. E. Coulon, M. Fanciulli, *Microelectron. Eng.* **85** (2008) 2411.

81. J. Päiväsaari, J. Niinistö, K. Arstila, K. Kukli, M. Putkonen, L. Niinistö, *Chem. Vap. Deposition* **11** (2005) 415.

82. W.-S. Kim, S.-K. Park, D.-Y. Moon, B.-W. Kang, H.-D. Kim, J.-W. Park, *J. Korean Phys. Soc.* **55** (2009) 590.

83. A.C. Jones, H.C. Aspinall, P.R. Chalker, R.J. Potter, K. Kukli, A. Rahtu, M. Ritala, M. Leskelä *Mater. Sci. Eng. B* **118** (2005) 97.

84. D.C. Bradley, J.S. Ghotra, F.A. Hart, *J. Chem. Soc., Dalton Trans.* (1973) 1021.

85. R.G. Gordon, J. Becker, D. Hausmann, S. Suh, *Chem. Mat.* **13** (2001) 2463.

86. W. He, S. Schuetz, R. Solanki, J. Belot, J. McAndrew, *Electrochem. Solid-State Lett.* **7** (2004) G131.

87. D. H. Triyoso, R. I. Hegde, J. Grant, P. Fejes, R. Liu, D. Roan, M. Ramon, D. Werho, R. Rai, L. B. La, J. Baker, C. Garza, T. Guenther, B. E. White Jr., P. J. Tobin, *J. Vac. Sci. Tech. B* **22** (2004) 2121.

88. D. H. Triyoso, R. I. Hegde, J. M. Grant, J. K. Schaeffer, D. Roan, B. E. White, Jr., P. J. Tobin, *J. Vac. Sci. Tech. B* **23** (2005) 288.

89. K. Kukli, M. Ritala, V. Pore, M. Leskelä, T. Sajavaara, R.I. Hegde, D.C. Gilmer, P.J. Tobin, A.C. Jones, H.C. Aspinall, *Chem. Vap. Dep.* **12** (2006) 158.

90. R. Inman, S.A. Schuetz, C.M. Silvernail, S. Balaz, P.A. Dowben, G. Jursich, J. McAndrew and J.A. Belot, *Mater. Chem. Phys.* **104** (2007) 220.

91. K. Kukli, M. Ritala, T. Pilvi, T. Sajavaara, M. Leskelä, A.C. Jones, H.C. Aspinall, D.C. Gilmer, P.J. Tobin, *Chem. Mater.* **16** (2004) 5162.

92. A.C. Jones, H.C. Aspinall, P.R. Chalker, R.J. Potter, K. Kukli, A. Rahtu, M. Ritala, M. Leskelä, *J. Mater. Chem.* **14** (2004) 3101.

93. Y. Luo, Y. Yao, Q. Shen, J. Sun, L. Weng, *J. Organomet. Chem.* **662** (2002) 144.

94. B.S. Lim, A. Rahtu, R.G. Gordon, *Nat. Mater.* **2** (2003) 749.

95. B.S. Lim, A. Rahtu, J.-S. Park, R.G. Gordon, *Inorg. Chem.* **42** (2003) 7951.

96. P. de Rouffignac, A.P. Yousef, K.H. Kim, R.G. Gordon, *Electrochem. Solid-State Lett.* **9** (2006) F45.

97. P. de Rouffignac, J.-S, Park, R.G. Gordon, *Chem, Mater.* **17** (2005) 4808.

98. J. Päiväsaari, C.L. Dezelah, D. Back, H.M. El-Kaderi, M.J. Heeg, M. Putkonen, L. Niinistö, C.H. Winter, *J. Mater. Chem.* **15** (2005) 4224.

99. A.P. Milanov, K. Xu, A. Laha, E. Bugiel, R. Ranjith, D. Schwendt, J. Osten, H. Parala, R. Fischer, A. Devi, *J. Am. Chem. Soc.* **132** (2010) 36.

100. X.L. Li, D. Tsoutsou, G. Scarel, C. Wiemer, S.C. Capelli, S.N. Volkos, L. Lamagna, M. Fanciulli, *J. Vac. Sci. Technol. A* **27** (2009) L1.

101. E.-J. Lee, M.-G. Ko, B.-Y. Kim, S.-K. Park, H.-D. Kim, J.-W. Park, *J. Korean Phys. Soc.* **49** (2006) 1243.

102. Y.-K. Moon, S. Lee, J.-W. Park, D.-H. Kim, J.-H. Lee, C.-O. Jeong, *J. Korean Phys. Soc.* **55** (2009) 1906.

103. J. Päiväsaari, M. Putkonen, T. Sajavaara, L. Niinistö, *J. Alloys Compd.* **374** (2004) 124.

104. M. Bosund, K. Mizohata, T. Hakkarainen, M. Putkonen, M. Söderlund, S. Honkanen, H. Lipsanen, *Appl. Surf. Sci.* **256** (2009) 847.

105. M. Malvestuto, G. Scarel, C. Wiemer, M. Fanciulli, F. D'Acapito,, F. Boscherini, *Nucl. Instr. and Meth. in Phys. Res. B* **246** (2006) 90.

106. G. Scarel, E. Bonera, C. Wiemer, C. Tallarida. S. Spiga, M. Fanciulli, I.L. Fedushkin, H. Schumann, Y. Lebedenskii, *Appl. Phys. Lett.* **85** (2004) 630.

107. E. Durğun Özben, J.M.J. Lopes, M. Roeckerath, St. Lenk, B. Holländer, Y. Jia, D.G. Schlom, J. Schubert, S. Mantl, *Appl. Phys. Lett.* **93** (2008**)** 052902.

108. L. F. Edge, D. G. Schlom, S. Rivillon, Y. J. Chabal, M. P. Agustin, S. Stemmer, T. Lee, M. J. Kim, H. S. Craft, J.-P. Maria, M. E. Hawley, B. Holländer, J. Schubert, K. Eisenbeiser, *Appl. Phys. Lett.* **89** (2006) 062902.

109. P. Sivasubramani, T. H. Lee, M. J. Kim, J. Kim, B. E. Gnade, R. M. Wallace, L. F. Edge, D. G. Schlom, F. A. Stevie, R. Garcia, Z. Zhu, D. P. Griffis, *Appl. Phys. Lett.* **89** (2006) 242907.

110. J.M.J. Lopes, U. Littmark, M. Roeckerath, S. Lenk, J. Schubert, S. Mantl, A. Besmehn, *J. Appl. Phys.* **101** (2007) 104109.

111. J.M.J. Lopes, M. Roeckerath, T. Heeg, U. Littmark, J. Schubert, S. Mantl, Y. Jia, D. G. Schlom, *Microelectron. Eng.* **84** (2007) 1890.

112. A. Vincze, R. Luptak, K. Husekova, E. Dobrocka, K. Fröhlich, *Vacuum* **84** (2010) 170.

113. R. Thomas, P. Ehrhart, M. Roeckerath, S. Van Elshocht, E. Rije, M. Luysberg, M. Boese, J. Schubert, M. Caymax, R. Waser, *J. Electrochem. Soc.* **154** (2007) G147.

114. H. Wang, J.-J. Wang, R. Gordon, J.-S.M. Lehn, H. Li, D. Hong,, D.V. Shenai, *Electrochem. Solid-State Lett.* **12** (2009) G13.

115. K.H. Kim, D.B. Farmer, J.-S.M. Lehn, P.V. Rao, R.G. Gordon, *Appl. Phys. Lett.* **89** (2006) 133512.

116. M. Roeckerath, J.M.J. Lopes, E. Durğun Özben, C. Urban, J. Schubert, S. Mantl, Y. Jia, D.G. Schlom, *Appl. Phys. Lett.* **96** (2010) 013513.

117. J.M.J. Lopes, M. Roeckerath, T. Heeg, J. Schubert, U. Littmark, S. Mantl, A. Besmehn, P. Myllymäki, L. Niinistö, C. Adamo, D.G. Schlom, *ECS Trans.* **11** (2007) 311.

118. J.M.J. Lopes, M. Roeckerath, T. Heeg, E. Rije, J. Schubert, S. Mantl, V.V. Afanas'ev, S. Shamuilia, A. Stesmans, Y. Jia, D.G. Schlom, *Appl. Phys. Lett.* **89** (2006) 222909.

119. C. Adelmann, S. Van Elshocht, A. Franquet, T. Conard, O. Richard, H. Bender, P. Lehnen S. De Gendt, *Appl. Phys. Lett.* **92** (2008) 112902.

120. H. Ono, T. Katsumata, *Appl. Phys. Lett.* **78** (2001) 1832.

121. K.J. Eisentraut, R.E. Sievers, *J. Am. Chem. Soc.* **87** (1965) 5254.

122. *UniQuant Version 2 User Manual*, Omega Data Systems, Veldhoven, Netherlands, 1994.

123. V. Sammelselg, J. Aarik, A. Aidla, A. Kasikov, E. Heikinheimo, M. Peussa, L. Niinistö, *J. Anal. At. Spectrom.* **14** (1999) 523.

124. M. Putkonen, T. Sajavaara, L. Niinistö, J. Keinonen, *Anal. Bioanal. Chem.* **382** (2005) 1791.

125. M. Ylilammi, T. Ranta-aho, *Thin Solid Films* **232** (1993) 56.

126. B. Klingenberg, M.A. Vannice, *Chem. Mater.* **8** (1996) 2755.

127. A.R. Teren, R. Thomas, J. He, P. Ehrhart, *Thin Solid Films* **478** (2005) 206.

128. E.P. Gusev, C. Cabral, M. Copel, C. D'Emic, M. Gribelyuk, *Microelectron. Eng.* **69** (2003) 145.

129. P. Myllymäki, J. Niinistö, M. Putkonen, M. Nieminen, L. Niinistö, *AVS 5th International Conference on Atomic Layer Deposition*, San Jose, USA, 2005, Extended Abstracts on CD-ROM.

130. C.L. Dezelah, IV, J. Niinistö, K. Arstila, L. Niinistö, C.H. Winter, *Chem. Mater.* **18** (2006) 471.

131. E.H. Nicollian, J.R. Brews, *MOS (Metal Oxide Semiconductor) Physics and Technology*, Wiley, New York, 1982, p. 465-466.